NATIONAL ENERGY TECHNOLOGY LABORATORY

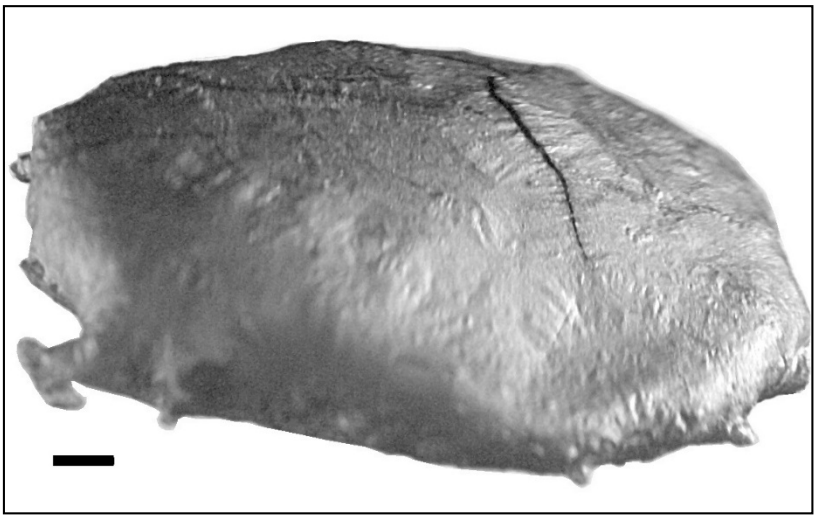

Detection of Hydrates on Gas Bubbles during a Subsea Oil/Gas Leak

22 July 2015

U.S. DEPARTMENT OF ENERGY

Office of Fossil Energy

NETL-TRS-6-2015

Disclaimer

This report was prepared as an account of work sponsored by an agency of the United States Government. Neither the United States Government nor any agency thereof, nor any of their employees, makes any warranty, express or implied, or assumes any legal liability or responsibility for the accuracy, completeness, or usefulness of any information, apparatus, product, or process disclosed, or represents that its use would not infringe privately owned rights. Reference therein to any specific commercial product, process, or service by trade name, trademark, manufacturer, or otherwise does not necessarily constitute or imply its endorsement, recommendation, or favoring by the United States Government or any agency thereof. The views and opinions of authors expressed therein do not necessarily state or reflect those of the United States Government or any agency thereof.

Cover Illustration: A high-resolution image showing a hydrate shell on a methane bubble during an experiment in the National Energy Technology Laboratory (NETL) High Pressure Water Tunnel Facility (HWTF) located in Pittsburgh, PA. Scale bar is 1 mm.

Suggested Citation: Levine, J. S.; Haljasmaa, I.; Lynn, R.; Shaffer, F.; Warzinski, R. P. *Detection of Hydrates on Gas Bubbles during a Subsea Oil/Gas Leak*; NETL-TRS-6-2015; EPAct Technical Report Series; U.S. Department of Energy, National Energy Technology Laboratory: Pittsburgh, PA, 2015; p 44.

An electronic version of this report can be found at:

http://www.netl.doe.gov/research/on-site-research/publications/featured-technical-reports

https://edx.netl.doe.gov/offshore

Detection of Hydrates on Gas Bubbles during a Subsea Oil/Gas Leak

Jonathan S. Levine[1], Igor Haljasmaa[2], Ronald Lynn[1], Frank Shaffer[1], Robert P. Warzinski[1]

[1] U.S. Department of Energy, National Energy Technology Laboratory, 626 Cochran Mill Road, Pittsburgh, PA 15236

[2] URS Corporation, National Energy Technology Laboratory, 626 Cochran Mill Road, Pittsburgh, PA 15236

NETL-TRS-6-2015

22 July 2015

NETL Contacts:

Robert P. Warzinski, Principal Investigator

Kelly Rose, Technical Coordinator

Cynthia Powell, Area Lead

This page intentionally left blank.

Table of Contents

EXECUTIVE SUMMARY **1**
1. INTRODUCTION **2**
1.1 BACKGROUND 2
1.2 RESEARCH PROGRAM 4
1.3 PROJECT OVERVIEW 6
2. HYDRATES AND HYDRATE DETECTION DURING AN OIL/GAS LEAK **7**
3. METHODS **10**
3.1 HIGH PRESSURE WATER TUNNEL FACILITY 10
3.2 EXPERIMENTS: BUBBLE PLUMES AND SINGLE BUBBLES 11
3.3 BUBBLE IMAGING AND AUTOMATED IMAGE ANALYSIS 11
4. OBSERVATIONS **12**
4.1 HYDRATE VISUAL DETECTION 12
4.2 QUANTITATIVE VIDEO ANALYSIS 21
4.3 CHEMICAL DETECTION METHODS 27
4.4 FUTURE DETECTION METHODS 30
4.5 FUTURE WORK: THERMODYNAMICS 31
5. CONCLUSIONS **33**
6. REFERENCES **35**

This page intentionally left blank.

List of Figures

Figure 1: The role of hydrates during a hydrocarbon leak..... 3
Figure 2: An overview of transport processes as an oil/gas hydrocarbon plume rises through the ocean. 5
Figure 3: Results of bubble plume model simulations by Dr. Ira Leifer, UCSB..... 6
Figure 4: An image of the Deepwater Horizon leak after the riser was cut. Annotations show how particle imaging velocimetry was performed using hydrate or wax particles.. 7
Figure 5: Fluids leaked from many different locations and leak geometries during Deepwater Horizon. 7
Figure 6: Gas exiting a leak passes through five phases (I-V) for the purposes of hydrate detection. 8
Figure 7: Photograph and process instrumentation diagram of the High Pressure Water Tunnel Facility (HWTF). 10
Figure 8: The presence of hydrate is clearly visible on the surface of the methane bubble on the right compared to the same bubble with no hydrates on the left. 12
Figure 9: Methane bubbles (Phase V) seen through the 4 cm window of the HWTF are about 4–10 mm diameter.. 13
Figure 10: Hydrates are clearly visible on methane bubbles in the HWTF. The hydrate-covered bubbles (Phase III) are seen through the 4 cm window of the HWTF and are about 7–10 mm diameter..... 14
Figure 11: A hydrate-covered methane bubble at successively lower pressures..... 14
Figure 12: A sequential series of images showing the rotation of a partially hydrate-covered 6.5-mm diameter methane bubble (Phase IV)..... 15
Figure 13: Bubble plumes in the HWTF (Phases I–II)..... 16
Figure 14: During Phase I, dense bubble plumes are optically difficult. The bright spots on each bubble are reflections of the side and back lighting off of other nearby bubbles. A hydrate covered bubble is hiding in the top right corner of the image at right..... 16
Figure 15: Bubbles are often out of focus in videos of dense bubble plumes simulating Phase I.17
Figure 16: During Phase II, dense bubble plumes have thinned out and only a handful of bubbles are visible creating ideal conditions for hydrate identification. Hydrate can be seen in all four images..... 18
Figure 17: A hydrate flake shedding from a methane bubble..... 19
Figure 18: A large hydrate flake in the HWTF..... 19
Figure 19: Three images of hydrates sticking to the upper surface of the HWTF viewing window cutout in a tapered plastic insert used for flow conditioning (see Section 3.1). 20
Figure 20: A hydrate cluster formed from many smaller gas bubbles in the HWTF metal cup used to collect small gas bubbles to form larger gas bubbles for HWTF single bubble experiments. 20
Figure 21: Gray-scale values change due to hydrate formation: the hydrate-free bubble is nearly black while the hydrates appear gray from reflected light..... 21
Figure 22: Methane bubbles covered in hydrate..... 22
Figure 23: A hydrate-covered bubble with a very jagged perimeter. 22
Figure 24: The ratio of the actual perimeter to the perimeter of an ideal ellipse vs. bubble size for bubbles with and without hydrate. 23
Figure 25: Rise velocity decreases approximately 10% after hydrate formation 24

List of Figures (continued)

Figure 26: Preliminary results indicate that small hydrate-covered bubbles (<2.5 mm) have significantly decreased rise velocities. 24
Figure 27: A sequential series of images showing one rotation of a 9-mm diameter oblate spheroid methane bubble. 25
Figure 28: A sequential series of images showing half a rotation of a 6-mm diameter oblate spheroid methane bubble. 25
Figure 29: A sequential series of images showing the rotation of a hydrate-covered 7-mm diameter methane bubble. 26
Figure 30: The maximum Allan variance, σA, of time-series bubble radius data decreases as the bubble size decreases for hydrate-free bubbles. 27
Figure 31: In the absence of hydrate, the solubility of each gas is independent. By contrast, hydrate dissolving into the ocean has a single fixed solubility controlled by the least soluble hydrate-former when corrected for the relative molar concentration in the hydrate. 28
Figure 32: Aqueous solubility of methane calculated with NETL-WVU's thermodynamic model: above the black vapor-liquid water-hydrate (VLH) curve the solubility is controlled by hydrate in equilibrium with water, below the curve hydrate is thermodynamically unstable and the solubility is controlled by gas solubility. 29
Figure 33: Aqueous solubility of a hydrocarbon mixture corresponding to the ratio of methane, ethane, and propane reported for Deepwater Horizon, and used as an illustrative ratio of light hydrocarbons. 30

Acronyms, Abbreviations, and Symbols

Term	Description
2-D	Two-dimensional
3-D	Three-dimensional
AUV	Autonomous underwater vehicle
BSEE	Bureau of Safety and Environmental Enforcement
CARS	Coherent anti-stokes Raman scattering
DOE	Department of Energy
EPAct	Energy Policy Act
HWTF	High Pressure Water Tunnel Facility
NETL	National Energy Technology Laboratory
NOAA	National Oceanographic and Atmospheric Administration
PNNL	Pacific Northwest National Laboratory
ppm	Parts per million
ROV	Remotely operated vehicle
UCSB	University of California, Santa Barbara
VLH	Vapor-liquid water-hydrate equilibrium
WVU	West Virginia University

Acknowledgments

This work was completed as part of National Energy Technology Laboratory (NETL) research for the U.S. Department of Energy's (DOE) Complementary Research Program under Section 999 of the Energy Policy Act of 2005.

This project benefited greatly from collaborations with Dr. Ira Leifer, University of California, Santa Barbara and Prof. Brian Anderson and Dr. Srinath Velaga, West Virginia University.

Experiments were performed with the assistance of Michael Schellhaas and Travis Kirby. High-frequency analysis of bubble hydrodynamics was performed with the assistance of Dr. Cantwell Carson. Insights into science for decision support and concerns regarding safety issues during a gas/oil leak owe much to discussions with Dr. C. J. Beegle-Krause, formerly with NOAA and currently at SINTEF. The potential for subsea Raman spectroscopy for this application benefited from discussions with Prof. Nancy Levinger, Colorado State University, Drs. George Bonheyo and Eric Winder, PNNL, and especially Drs. Michael Buric, Dustin McIntyre, and Steven Woodruff, NETL-Morgantown.

The authors wish to acknowledge Roy Long (NETL Strategic Center for Natural Gas and Oil) and Elena Melchert (DOE Office of Fossil Energy) for programmatic support.

EXECUTIVE SUMMARY

Laboratory experiments at the National Energy Technology Laboratory (NETL) High Pressure Water Tunnel Facility (HWTF), located in Pittsburgh, PA, have enabled high-speed videography of hydrate on hydrocarbon gas bubbles. An extensive set of several hundred experiments produced unprecedented high-fidelity images that have shown previously unknown hydrate morphologies with complex linkages to bubble hydrodynamics and complex surface behavior. Hydrate is clearly visible in high-speed, high-definition video at the HWTF. During a deepsea blowout a human would easily be able to identify hydrate on 2–10 mm diameter bubbles. However, image quality is critical and requires the design of a deepsea video system in advance of any leak. Results from quantitative automated image analysis developed during this project point to several indicators of the presence of hydrate including gray-scale values, rise velocity, and high-frequency hydrodynamic/shape analysis.

Future work points to the need for liquid water-hydrate thermodynamic measurements of hydrocarbon mixtures as well as hydrocarbon/sour gas mixtures. This would enable further development of the predictive hydrate thermodynamic model created for this project by collaborators at West Virginia University (WVU) to include hydrogen sulfide. Development of a coherent anti-stokes Raman scattering (CARS) and waveguide-enhanced Raman spectroscopy system would enable deepsea hydrate quantification and subsea hydrocarbon detection. Such a system would also enable laboratory determination of hydrate skin composition, provide data necessary for modeling the dissolution of mixed hydrocarbon bubbles, and support thermodynamic measurements. This type of information is essential to developing predictive models that can show, for example, when dispersant application is necessary to reduce the risk of flammable or toxic gases from reaching the ocean surface.

1. INTRODUCTION

1.1 BACKGROUND

The formation of clathrate hydrates can create a variety of challenges during the response to a leaking oil/gas well (Figure 1). For example, hydrates plugged the initial containment dome deployed to pull up leaking gas and oil during the 2010 Deepwater Horizon Macondo well disaster. Clathrate hydrates are a crystalline solid composed of hydrogen-bonded water encaging ("enclathrating") hydrate-forming molecules. In hydrocarbon systems these molecules are typically the lighter alkanes, sour gases, and their mixtures: methane, ethane, propane, isobutane, carbon dioxide, and hydrogen sulfide. At the high pressures of the deepsea, clathrate hydrates of light alkanes and sour gases are thermodynamically stable at temperatures above those required for ice formation. Therefore, the lighter components of a leaking hydrocarbon mixture can form solid clathrate hydrate after contact with cold, deep-sea water, either as free-floating solid hydrate particles or as hydrate skins on the surface of gas bubbles. The hydrate will then slowly dissolve into the ocean due to the slight solubility of hydrocarbons in seawater or will melt upon rising to shallower water where hydrates are thermodynamically unstable due to reduced hydrostatic pressure and typically warmer temperatures.

Hydrates are of concern for several very different reasons during a deep-sea oil/gas leak. The best-known concern is plugging of equipment being used to respond to a leak, whether the caisson deployed during Deepwater Horizon or flowlines used to pull a hydrocarbon/water mixture up to the surface. This is a routine problem that must be avoided or managed during deepwater hydrocarbon production where it is termed flow assurance (Sloan and Koh, 2008; Sloan et al., 2010). Hydrate detection inside and around production-related equipment is being studied by industry, e.g. Anderson et al. (2012).

Away from the immediate vicinity of production equipment, leaking oil and gas create a different set of concerns: safety, fate, and economic/environmental damage. Hydrates can play a critical role enabling transport of leaking hydrocarbons through the deepsea to shallower depths as well as to the sea surface (Section 1.2). Flammable light alkanes and toxic hydrogen sulfide have the potential to pose a safety hazard to responding personnel and equipment. Subsea transport of hydrocarbons to the surface have caused operational safety concerns during previous subsea leak responses, e.g., while not involving hydrates, the shallow 1979 Ixtoc blowout required operations at a safe distance from a surface fire and a 2012 gas leak at the Elgin field required the evacuation of personnel from several production platforms (Werdigier and Fountain, 2012).

Another danger is posed by toxic hydrogen sulfide. Hydrogen sulfide would ordinarily be expected to rapidly dissolve in the ocean due to its high aqueous solubility. However, dissolution of hydrate-covered bubbles is set by the solubility of the least-soluble hydrate former weighted by hydrate composition (Section 1.2). Therefore, a hydrate shell composed of a hydrocarbon-hydrogen sulfide mixture may enable hydrogen sulfide transport to the sea surface.

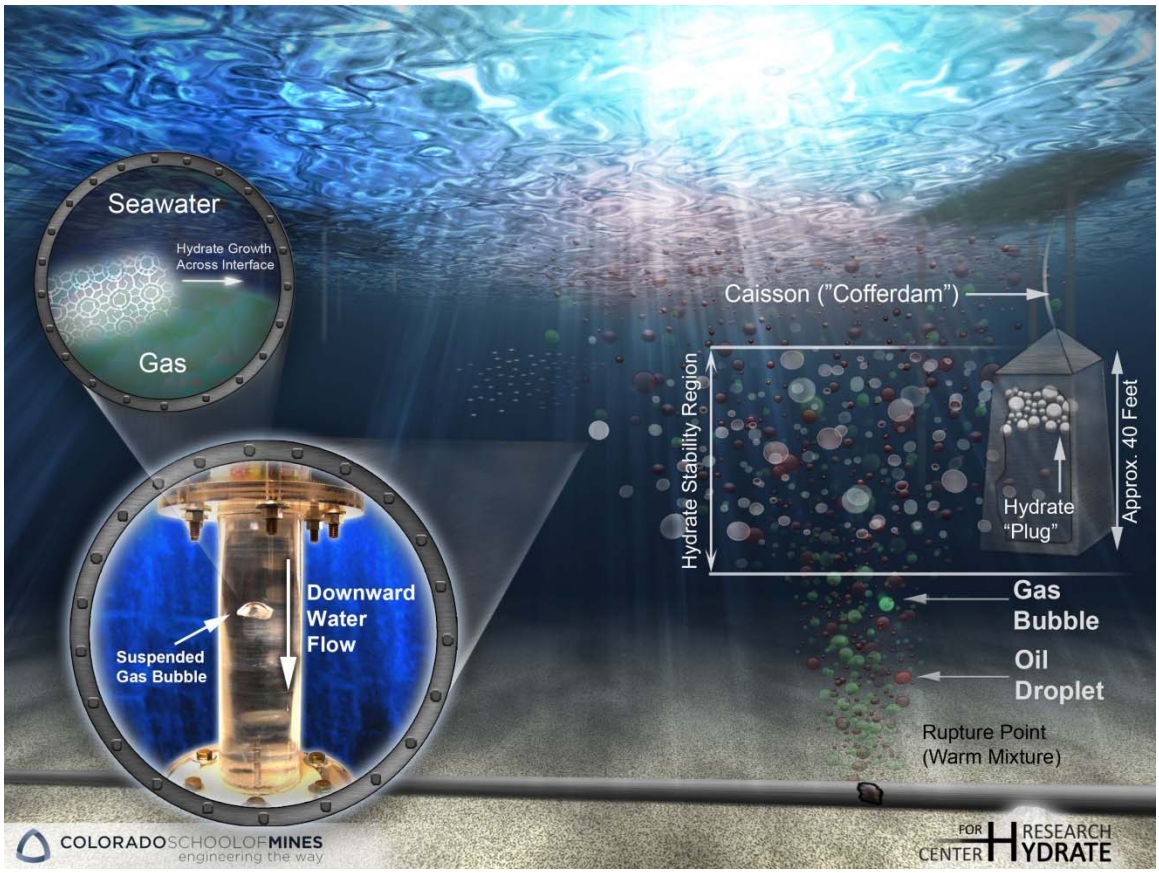

Figure 1: The role of hydrates during a hydrocarbon leak.

Bottom right: Warm leaking gas and oil buoyantly rises through the ocean, cooling off from contact with cold deepsea water. Light alkanes and sour gases can form hydrate at the high pressures and cold temperatures of the deepsea.

Right: Hydrate formation can plug equipment being used to pull up leaking hydrocarbons such as the caisson deployed during the Deepwater Horizon response.

Center: The formation of hydrate shells reduces the dissolution rate of buoyantly rising gas bubbles, resulting in their transport to shallower depths and potentially the sea surface. If flammable hydrocarbons or toxic hydrogen sulfide reach the surface they pose a safety risk to responding personnel.

Left: Laboratory experiments require suspending buoyantly rising gas bubbles with downward flowing water to achieve the longer experimental times necessary to study relevant hydrate processes. Hydrate formation requires both gas and water and therefore forms at the surface of bubbles.

Image courtesy of Dr. Zachary Aman, formerly Center for Hydrate Research, Colorado School of Mines.

Modeling the short- and long-term fate of leaking hydrocarbons requires an accurate understanding of deep-sea bubble and bubble plume transport including reduced dissolution rates and rise velocities due to hydrate formation (Section 1.2). An accurate understanding of hydrocarbon transport is necessary to predict the effects of actions taken during a spill response,

e.g. subsea dispersant release. If hydrate formation further modifies the surfactant-altered chemical or physical properties of rising hydrocarbons, the net result would be to alter the subsea depth of hydrocarbon intrusion layers. Differences in current direction between the original and modified intrusion depths would then transport hydrocarbons in different directions, ultimately resulting in exposure to different ecosystems (Adams, 2011).

Finally, hydrate detection during deep-sea leaks is important in establishing public confidence in the response technology. The Department of Commerce's National Oceanographic and Atmospheric Administration (NOAA) reports that during previous leaks real economic damage has resulted from misunderstanding resulting from inadequate communication of technical data to the public, i.e. "rivers of oil" never reached beaches, but the perception nonetheless caused the cancellation of vacations and other commerce (NOAA , 2011).

Thus, detection of hydrates on deepsea gas bubbles provides important information at all stages of a response, from immediate decision-support for responding personnel concerned with safety and controlling the leaking hydrocarbons, to longer-term modeling of pollutant fate and thus environmental damage.

1.2 RESEARCH PROGRAM

The U.S. Department of Energy's (DOE) Complementary Research Program under Section 999 of the Energy Policy Act of 2005 (EPAct) funded research reported here was facilitated by complementary funding from the former Bureau of Ocean Energy Management, Regulation and Enforcement, now the Bureau of Safety and Environmental Enforcement (BSEE). An extensive set of experiments, primarily in the National Energy Technology Laboratory (NETL) High Pressure Water Tunnel Facility (HWTF), were performed to measure fundamental properties related to hydrate formation on hydrocarbon bubbles transiting the oceanic water column. A comprehensive set of several hundred experiments on single bubbles at pressures and temperatures spanning the deep ocean measured: (1) dissolution rates; (2) rise velocities; (3) hydrodynamic behavior; (4) hydrate formation/melting thermodynamic conditions; (5) hydrate onset times and growth rates; and (6) hydrate features from high-resolution, high-speed videos. Experiments were performed with methane and a mixture of 87.5% methane, 8.1% ethane, and 4.4% propane.

If not captured at or near the point of leakage, hydrocarbons and sour gases will rise toward the sea surface. Laboratory experiments at NETL's HWTF have shown that hydrate shells on the exterior of gas bubbles greatly reduce dissolution rates, with hydrate solubility controlling dissolution rather than gas solubility (Warzinski et al., 2014b). Field experiments show that hydrate formation results in gas transport to shallower depths and in some cases transport to the sea surface (Rehder et al., 2009; Solomon et al., 2009).

Dr. Ira Leifer, of University of California, Santa Barbara (UCSB), has updated his deep-sea bubble and plume transport model (Figure 2) based on insights from dissolution experiments at the HWTF showing that hydrate-covered bubble dissolution is set by aqueous-phase hydrate solubility (MacDonald, 2011). Collaborators Prof. Brian Anderson and Dr. Srinath Velaga, of West Virginia University (WVU), have developed a thermodynamic model capable of accurately predicting the aqueous solubility and thermodynamic stability of light alkane hydrates in the deepsea (Velaga, 2014) that has been incorporated in the bubble/plume model (Figure 2 and Figure 3). The updated deep-sea hydrocarbon transport model accurately reproduces field data

showing hydrocarbon transport to the sea surface, while also showing that the depths of enhanced light alkane layers correspond to predicted pressures for hydrate melting (MacDonald, 2011). Additional details of these results are currently being incorporated into reports to BSEE as well as other manuscripts for publication.

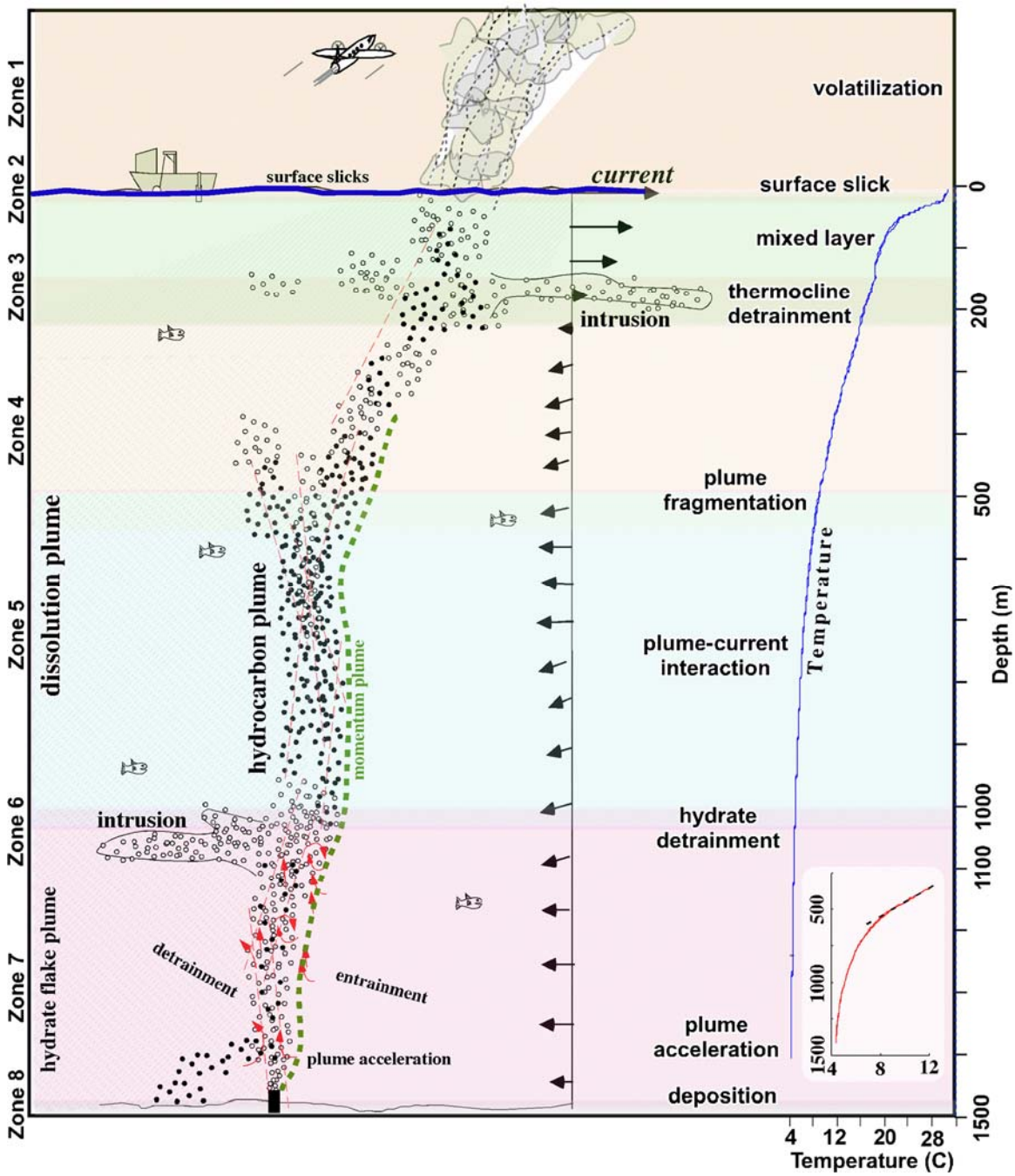

Figure 2: An overview of transport processes as an oil/gas hydrocarbon plume rises through the ocean. (Courtesy of Dr. Ira Leifer, UCSB)

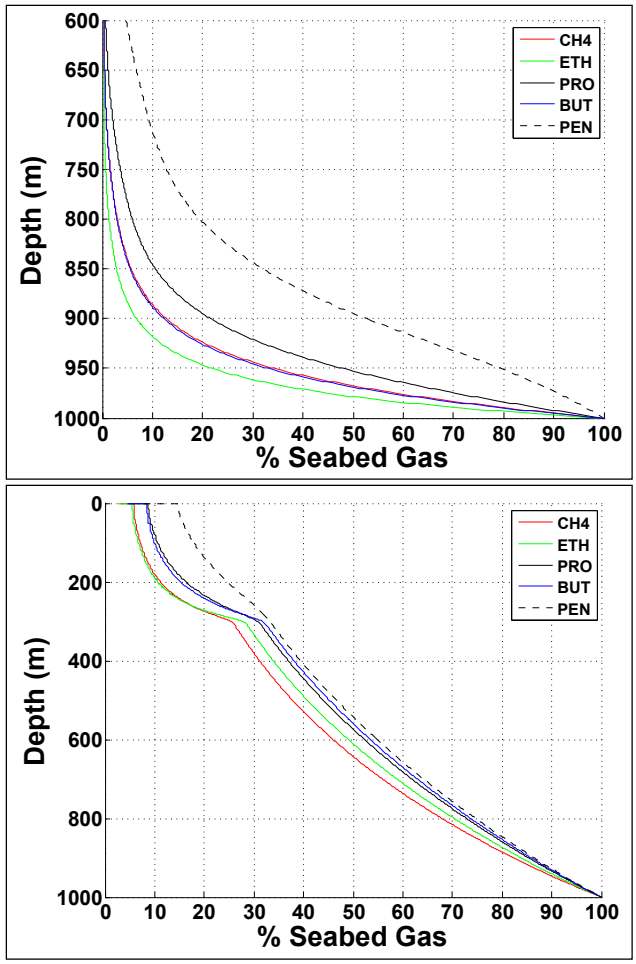

Figure 3: Results of bubble plume model simulations by Dr. Ira Leifer, UCSB.

Left: Modeling results without hydrates, i.e. aqueous solubility is set by the hydrocarbon phase. Gas bubbles rapidly dissolve into the deepsea in the absence of hydrates.

Right: Modeling with hydrates shows reduced aqueous solubility results in hydrocarbon transport to the sea surface. Bubble dissolution is limited by the dissolution of a surface layer of hydrate melting into the surrounding water, i.e. aqueous solubility is set by the hydrate phase. Hydrate becomes thermodynamically unstable due to depressurization and complete dissociation causes enhanced dissolution at ~300 m for this particular natural gas mixture. Bubble gas now makes it to the sea surface.

1.3 PROJECT OVERVIEW

This report aims to provide insights into deep-sea hydrate detection during an oil/gas leak based on laboratory experiments at the NETL HWTF comparing properties of gas bubbles with and without hydrate at deep-sea conditions. The presence of hydrates on the surface of a rising gas bubble can be detected by a variety of visual and computer vision methods. Additionally, lessons from this project point to several field-relevant measurement techniques for hydrate detection.

2. HYDRATES AND HYDRATE DETECTION DURING AN OIL/GAS LEAK

The possibilities for hydrate detection from a remotely operated vehicle (ROV) will change as hydrocarbons are diluted as they move from a leak through the ocean toward the surface. At the point of leakage fluids may be in the turbulent jet phase where hydrate identification will require entirely different techniques than those discussed here, see Figure 4.

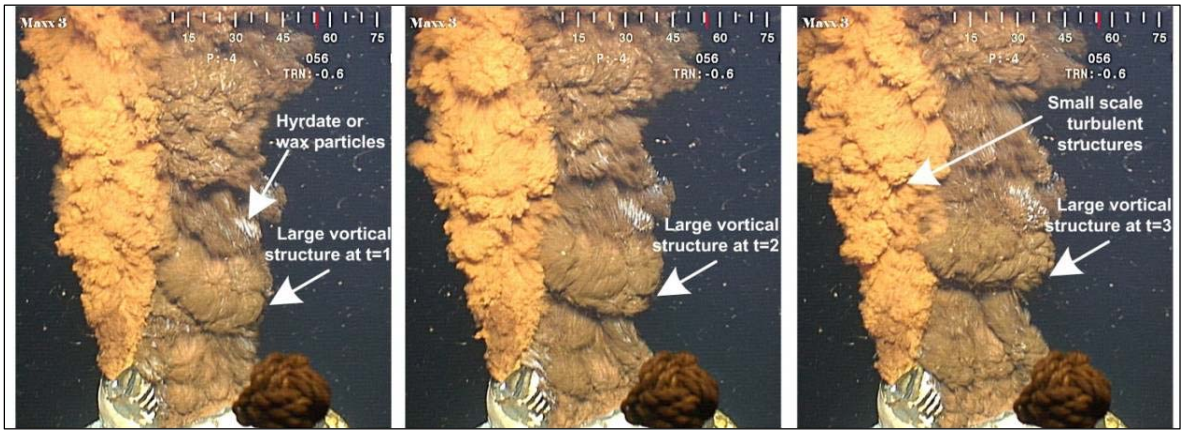

Figure 4: An image of the Deepwater Horizon leak after the riser was cut. Annotations show how particle imaging velocimetry was performed using hydrate or wax particles. Image courtesy of Frank Shaffer, NETL, originals from BP video during the Deepwater Horizon Macondo well disaster.

It is not possible to determine if the white specks in Figure 4 were hydrate or some other solid such as wax. The leaking fluids were reported to be too warm for hydrate formation, i.e., hydrates should not have been thermodynamically stable inside the hot jet. This would not necessarily have been true before the riser was cut when fluids could have cooled as they flowed through the riser along the seafloor, see Figure 5.

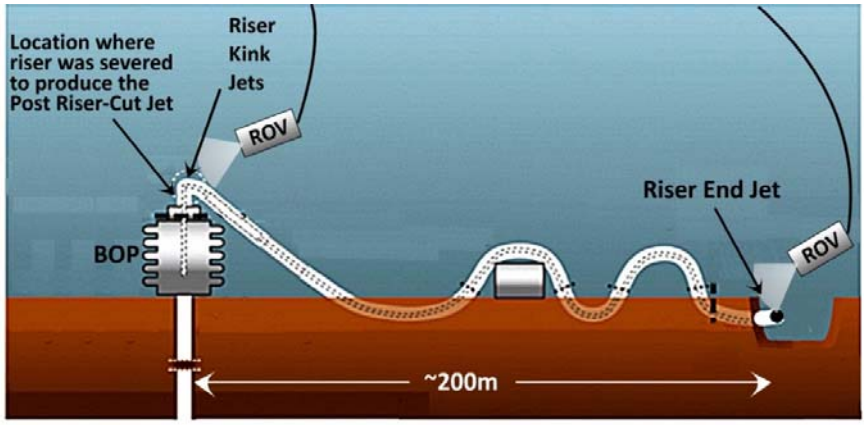

Figure 5: Fluids leaked from many different locations and leak geometries during Deepwater Horizon. Image modified by Frank Shaffer, NETL, original BP.

Future leaks could result in a wide variety of scenarios with different flow paths and leak geometries producing different thermal and fluid mixing. Purposeful chemical or physical modifications such as spraying dispersants or other chemicals into leaking fluids would further alter conditions in the vicinity of a leak. As a result, leaking gas and oil may enter the ocean at many different conditions relevant to hydrate formation with variations in parameters such as temperature, droplet and bubble size distribution, and oil/gas to water ratio. For example, compare the high-momentum fine spray from the riser kink jets with the low-momentum riser end jet. Therefore at the point of the leak hydrate formation could be completely impossible, e.g. a hot hydrocarbon jet lacking any water, or nearly assured, e.g. a cold stationary water-filled metal box accumulating gas. Therefore, reliable hydrate detection in the immediate vicinity of a leak including the momentum-drive jet regime is expected to be much more difficult than in the far field.

Outside the momentum-driven jet, leaking hydrocarbons will become increasingly dilute, transitioning from a dense set of hydrocarbon bubbles with many bubble-bubble interactions near the leak, to a sparse set of non-interacting bubbles after sufficient water is entrained in the far field, see Figure 6.

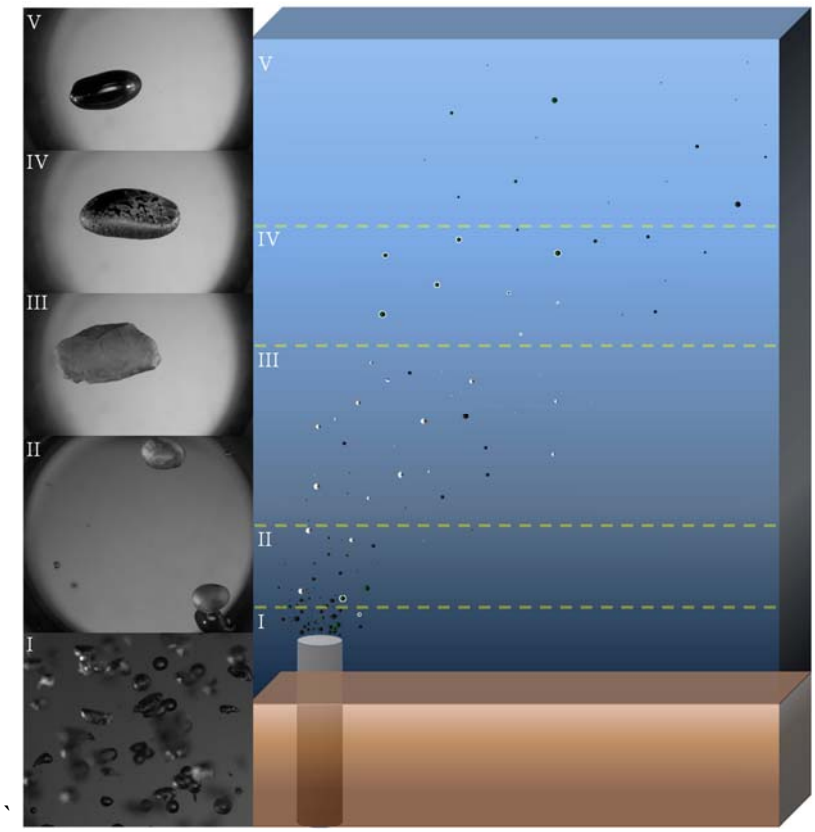

Figure 6: Gas exiting a leak passes through five phases (I-V) for the purposes of hydrate detection. See descriptions of each phase in the text below. Different experiments are required to reproduce the conditions in each phase, see Section 3.2 below.

Phase I: The momentum-driven jet phase of a leak transitions to a dense field of buoyancy-driven individual gas bubbles and oil droplets. Bubble-bubble interaction can occur in this phase

and aqueous gas concentrations are elevated. Hydrate formation is most likely in this region owing to elevated gas concentrations and to lower temperatures beyond the immediate leak as cold deep-sea water is drawn into the jet. Phase I is characterized by optically dense fields of view that will be challenging for automated video analysis.

Phase II: Bubbles begin to spread out. If hydrates were to form they would be expected to form by Phase II. Unlike Phase I, bubble-bubble interactions will be minimal and automated image analysis of single bubbles is possible. Bubble detection by an ROV would be possible.

Phase III: Bubble interactions do not occur in this phase. Observation in this phase should be straightforward.

Phase IV: Bubbles approach and transit the vapor-liquid water-hydrate (VLH) thermodynamic equilibrium hydrate. The hydrate skins begin to melt and will only partially cover solitary gas bubbles. The hydrate completely melts near the VLH equilibrium point. Typically Phase IV takes place in the thermocline.

Phase V: This phase is in the upper mixed ocean layer. Hydrates are not present. Hydrate formation is therefore only relevant in enabling hydrocarbon and sour gas transport to these shallow depths.

3. METHODS

3.1 HIGH PRESSURE WATER TUNNEL FACILITY

The NETL High Pressure Water Tunnel Facility (Figure 7) was designed to study the chemistry, physics, and hydrodynamics of rising gas bubbles at deep ocean conditions, simulating water depths to 3,400 m and temperatures down to freezing (Warzinski et al., 2004; Haljasmaa et al., 20005; Warzinski et al., 2008; Lynn et al., 2014). A vertical, countercurrent water flow is used to stabilize buoyant gas bubbles in a viewing window for minutes to hours while video-based measurements are made. A custom flow conditioner (Figure 7 inset) located upstream of the test section creates a velocity minimum near the vertical axis of the viewing section that provides radial stabilization. Tapered plastic inserts are also used to stabilize the bubble in the vertical direction. Bubbles up to about 20-mm diameter have sufficient freedom to permit a measure of natural hydrodynamics to be observed, in particular, wake-induced lateral path and shape oscillations. Critically, these systems allow bubbles to be stabilized for sufficiently long times to observe hydrate formation, while also preventing the bubbles from contacting the system walls, which would alter the hydrate formation process.

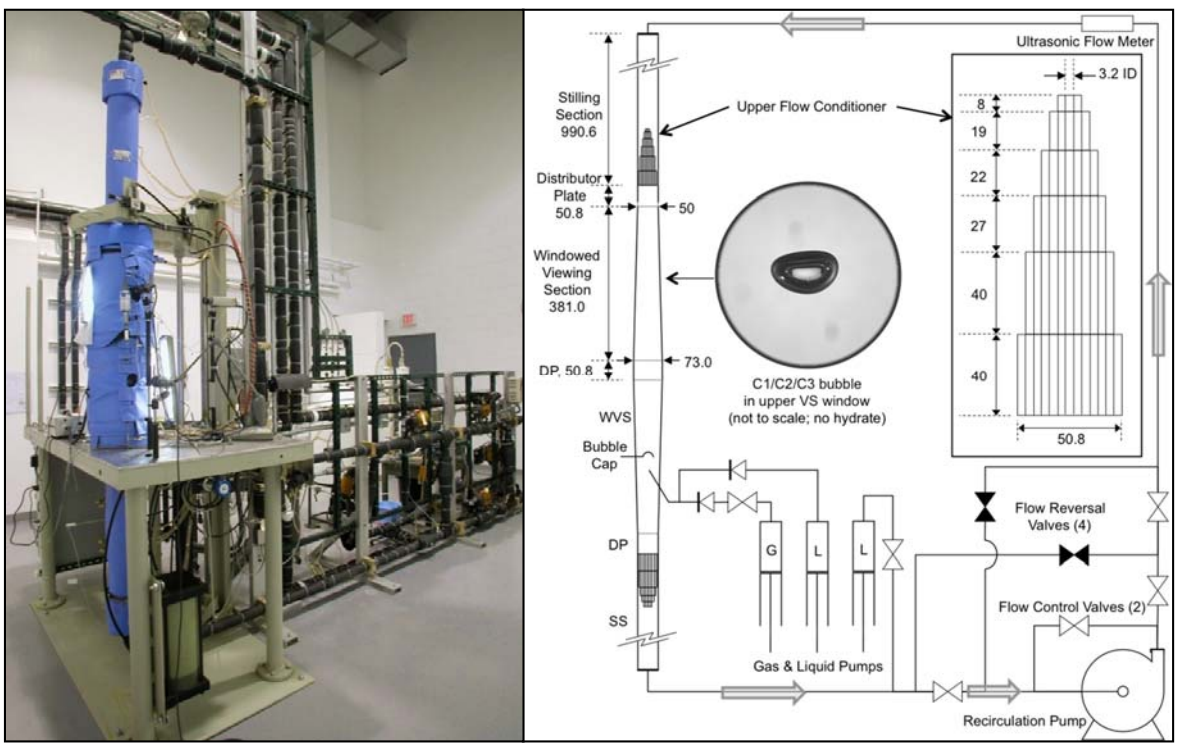

Figure 7: Photograph (left) and process instrumentation diagram (right) of the High Pressure Water Tunnel Facility (HWTF). Insets show (center right) an image of a non-hydrated bubble and (top right) the flow conditioner used to stabilize the bubble in the center of the tunnel.

The HWTF is controlled and monitored by a custom written LabVIEW virtual instrument. Bubble rise velocities are determined from the countercurrent flow used to stabilize each bubble

in the HWTF viewing window (Lynn et al., 2014). The system is actively controlled to ensure constant pressure and temperature conditions. Known quantities of hydrocarbon gas are injected into the system to set the aqueous-phase hydrocarbon concentration in each experiment. A protocol was developed to ensure that the system is well mixed between experiments to prevent hydrate nucleation elsewhere in the system. By accurately controlling the pressure, temperature, and aqueous-phase hydrocarbon concentration, the thermodynamic state of the system can be compared to predictions from WVU's hydrate thermodynamics model (Velaga, 2014). Because experiments are performed at a known thermodynamic state, the experimental results can be broadly applied to any deepsea condition, and insights regarding the role of hydrates and their detection during a deepsea blowout are broadly applicable.

3.2 EXPERIMENTS: BUBBLE PLUMES AND SINGLE BUBBLES

Experiments at the HWTF simulated bubble plumes and single bubbles representing Phases I-V. Bubble plumes simulating Phases I and II were simulated in the HWTF by releasing a known volume of gas into the HWTF to create a plume of many tens to hundreds of bubbles. Counterflowing water keeps the plume in the HWTF test section, though each individual bubble goes in and out of view many times. As more bubbles are lost the bubble density gradually decreases, simulating the transition from Phase I to Phase II. Bubble plumes are physically and chemically complicated due to complex wake structures and aqueous hydrocarbon concentration enhancements downstream of each bubble. By contrast, single bubble experiments have the advantage of being well constrained: physically, flow fields near single bubbles have been extensively studied, e.g. Clift, et al. (2005), Fan and Tsuchiya (1990); chemically, the bulk aqueous hydrocarbon concentration is the same throughout the HWTF. Phases III, IV, and V are simulated by releasing single bubbles at representative thermodynamic conditions, inside, at the border of, and outside the hydrate stability region respectively. Each single bubble experiment lasts many tens of minutes to hours, which is the time scale for a single bubble to rise through the ocean (Rehder, 2009).

3.3 BUBBLE IMAGING AND AUTOMATED IMAGE ANALYSIS

A Vision Research Phantom v341 high-speed camera was used to record both continuous high-definition video, 720 X 480 at 30 fps with 44 μm pixel resolution, and high-speed, higher-definition video, 2560 x 1680 at either 195 or 1000 fps with 12 μm pixel resolution. The former is a standard HD-SDI video signal, though the clarity of the HD-SDI images analyzed here benefit from the higher quality optics and CCD of the high-speed camera. The short exposure times for the high-speed video required adding significant external lighting to the HWTF.

The images presented in Section 4 are higher-resolution images taken at high speed during experiments in the HWTF, typically 195 fps. The unprecedented high fidelity of these images resulted in the discovery of surface hydrate morphologies similar to those found in sea ice (Warzinski et al., 2014b). The combination of both high-speed and high-resolution video enabled the identification of a dynamic coupling between surface hydrodynamics and hydrate morphology/thickness controlled by hydrate thermodynamic state (Warzinski et al., 2014b).

Automated extraction of bubbles from images for quantification has been performed in both ImageJ and LabVIEW (Warzinski et al., 2014b). Quantitative assessment of hydrate-induced changes to bubble surfaces and hydrodynamics was achieved using a custom automated vision analysis code written with LabVIEW (Warzinski et al., 2014a). Details are in Section 4.

4. OBSERVATIONS

4.1 HYDRATE VISUAL DETECTION

4.1.1 Visual Indicators of Hydrates

The difference between bubbles with and without hydrate are often easy to see in the high fidelity, 12 µm-resolution images taken at the HWTF as shown in (Warzinski et al., 2014b). During an oil/gas blowout a straightforward visual analysis may be possible during Phases II and III if the lighting is sufficient. This is discussed further in Section 4.1.5.

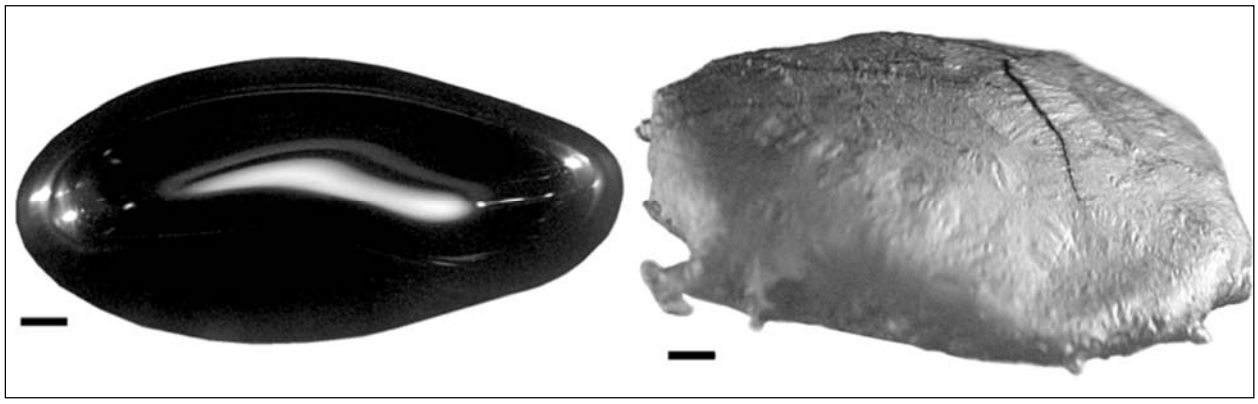

Figure 8: The presence of hydrate is clearly visible on the surface of the methane bubble on the right compared to the same bubble with no hydrates on the left. Each figure contains a 1-mm scale bar. (Warzinski et al., 2014b)

Observations are presented in the following sections in order of increasing complexity. Phase V, single bubbles with no hydrates, is the baseline for comparison purposes. This is contrasted with Phase III, hydrate completely covering single bubbles. Next, the more complex morphologies of Phase IV, single bubbles near the hydrate melting point that are either partially covered in hydrate or fully covered with a thin hydrate shell, may be more difficult to detect. Last is the more complicated case of many bubbles in a plume, i.e., Phase I transitioning to Phase II.

4.1.2 Visual Indicators of Hydrates on Single Bubbles

Methane bubbles without hydrate (Phase V) appear transparent to the eye, but appear mostly dark to the video camera (left image in Figure 8) because of the difference in index of refraction with the surrounding water. The bright regions in this image are due to lensing of the backlighting and reflections of side lighting.

The 4–10 mm diameter bubbles that can be stabilized for long periods of time in the HWTF are oblate spheroids. They appear as ellipses overlaid with surface capillary waves when viewed by a camera from the side (Figure 8 and Figure 9). As bubbles decrease in size, the effect of surface tension increases relative to the shape-distorting effects of buoyancy. As a result, as bubbles decrease in size they become more spherical (Figure 9), becoming nearly spherical below about 2-mm diameter.

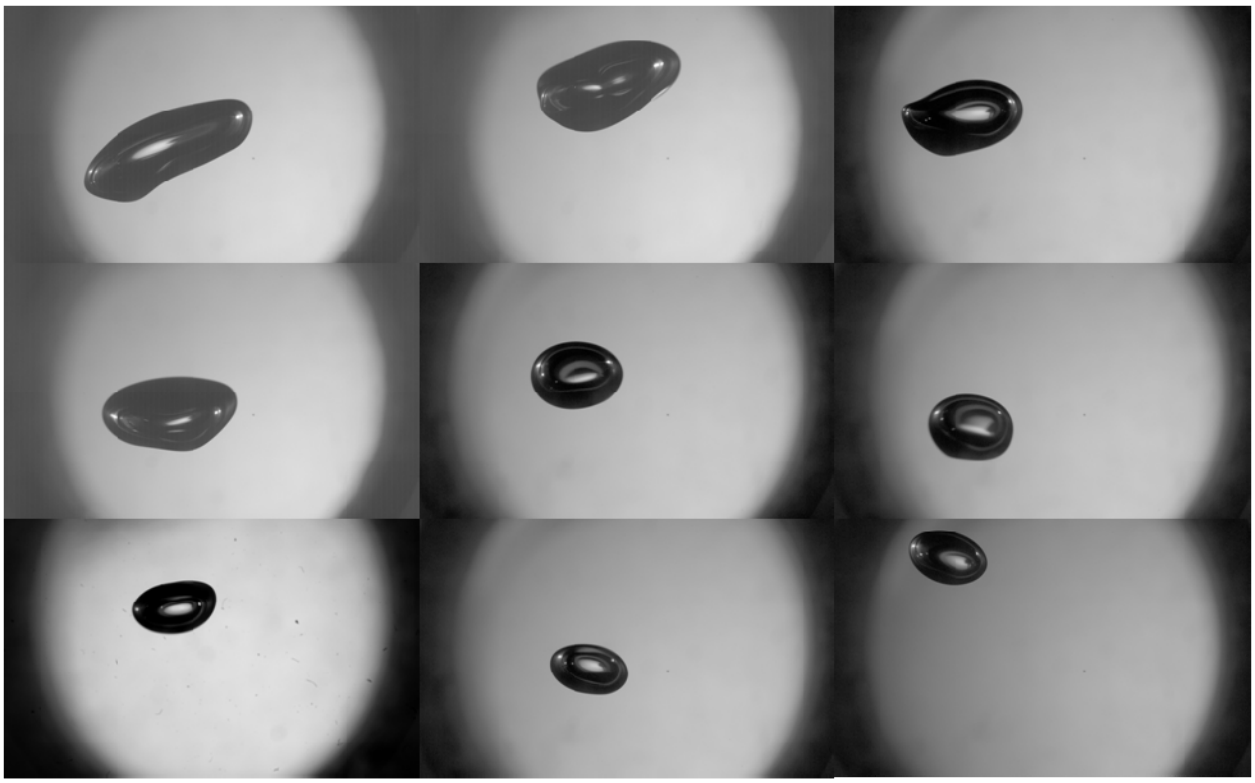

Figure 9: Methane bubbles (Phase V) seen through the 4 cm window of the HWTF are about 4–10 mm diameter. Bubbles in this size range are oblate spheroids and appear as ellipses modified by surface distortions. Surface distortions decrease as surface tension becomes more important at smaller sizes.

In contrast to a bubble with no hydrate, hydrate skins on single bubbles (Phase III) are similar in appearance to a snowy ice sheet, with complex topography casting shadows and other features that are distinguishable to the eye (Figure 8 and Figure 10). At high driving energies (Phase II-III), hydrate can grow into irregular shapes resembling icicles or other unusual shapes (Figure 10 and Figure 11). Hydrate is a solid crystal lattice of hydrogen-bonded water molecules encaging guest molecules and thus has many similarities to ice for visual identification purposes. Visually complex surface textures result from many different crystals growing on the surface of each bubble. Surficial hydrates have complex structures and morphologies that are similar in appearance to sea ice owing to comparable relationships between morphology and surface hydrodynamics (Figure 11) (Warzinski et al., 2014b).

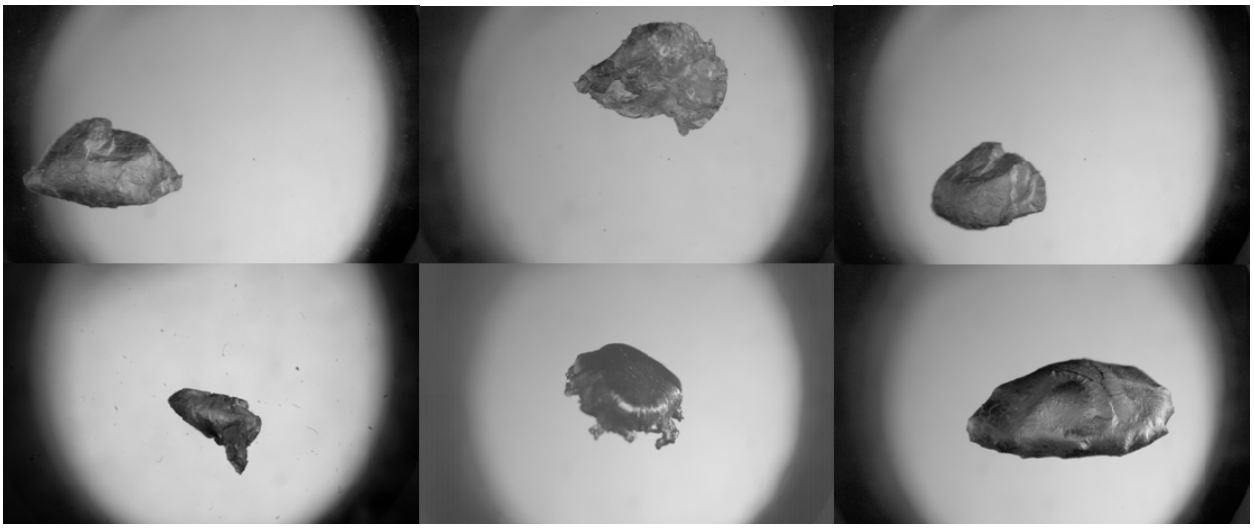

Figure 10: Hydrates are clearly visible on methane bubbles in the HWTF. The hydrate-covered bubbles (Phase III) are seen through the 4 cm window of the HWTF and are about 7–10 mm diameter.

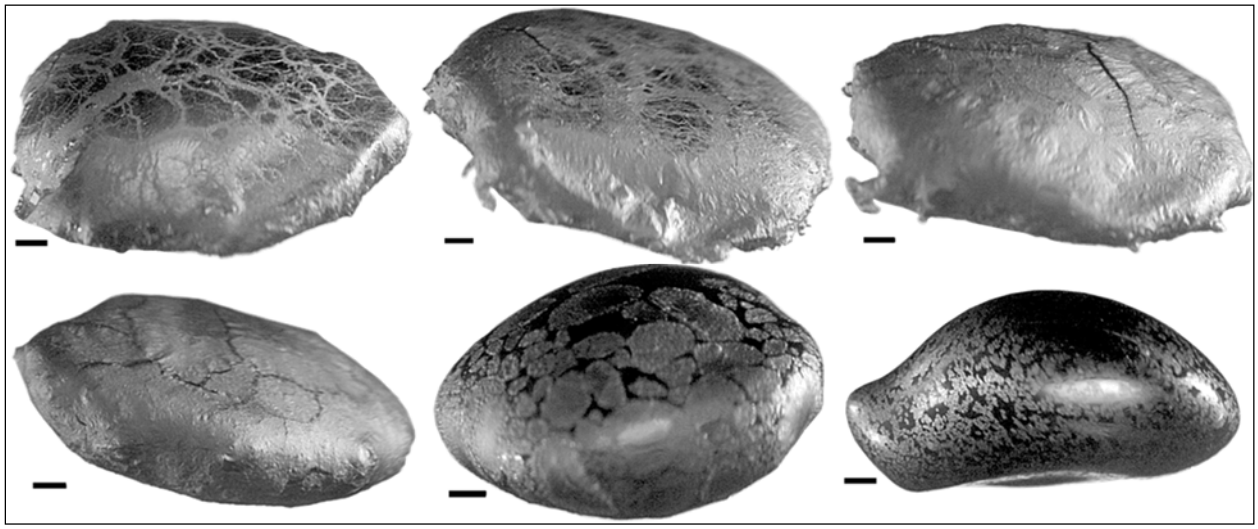

Figure 11: A hydrate-covered methane bubble at successively lower pressures; images are from and details are in Warzinski, et al. (2014a). Top: The hydrate shell is thicker and rougher at higher thermodynamic driving force resulting in irregular edges (Phase III). Bottom: As the bubble rises and pressure drops, reduction in thermodynamic driving force thins and breaks up the hydrate shell (Phase IV).

Hydrate detection during Phase IV, while hydrates are melting or near to melting, will be significantly more difficult since there will be less hydrate on each bubble and they will therefore be causing less overall effect (Figure 11). Furthermore, partial hydrate skins or thin translucent hydrate skins can be significantly more difficult to see (Figure 12). However, detection of hydrates in Phase IV will be less important because melting hydrates will have less of an effect on transport and thus hydrocarbon fate. The simplest solution in such cases is to send the measuring ROV to deeper depths at which thick hydrates will be more easily detectible. The

ROV can then be made to slowly ascend to identify the approximate depth of the beginning of Phase IV, which should correspond to the bottom of a hydrocarbon intrusion layer.

Figure 12: A sequential series of images showing the rotation of a partially hydrate-covered 6.5-mm diameter methane bubble (Phase IV). Hydrate can be difficult to impossible to detect, particularly in regions that are dark or out of focus.

4.1.3 Hydrates in Bubble Plumes

Hydrate detection in dense bubble plumes, Phase I, is made easier by the significantly increased number of bubbles and ease of ROV operation: the ROV can be located in the near vicinity of the leak rather than having to find millimeter to centimeter sized single bubbles transiting hundreds of meters of deep ocean. Figure 13 shows bubble plumes observed in the HWTF with and without hydrate. The human eye is able to identify the smooth perimeter and dark appearance of the bubbles without hydrate (top images), and the variations in surface texture of the hydrate-covered bubbles (bottom images). The hydrate covered bubbles vary by lighting and hydrate thickness: hydrates are white or gray and their perimeters are smooth in the bottom left and bottom right images in Figure 13, but in the bottom middle image they appear black with jagged features and flakes of hydrates can be seen detaching from their surfaces.

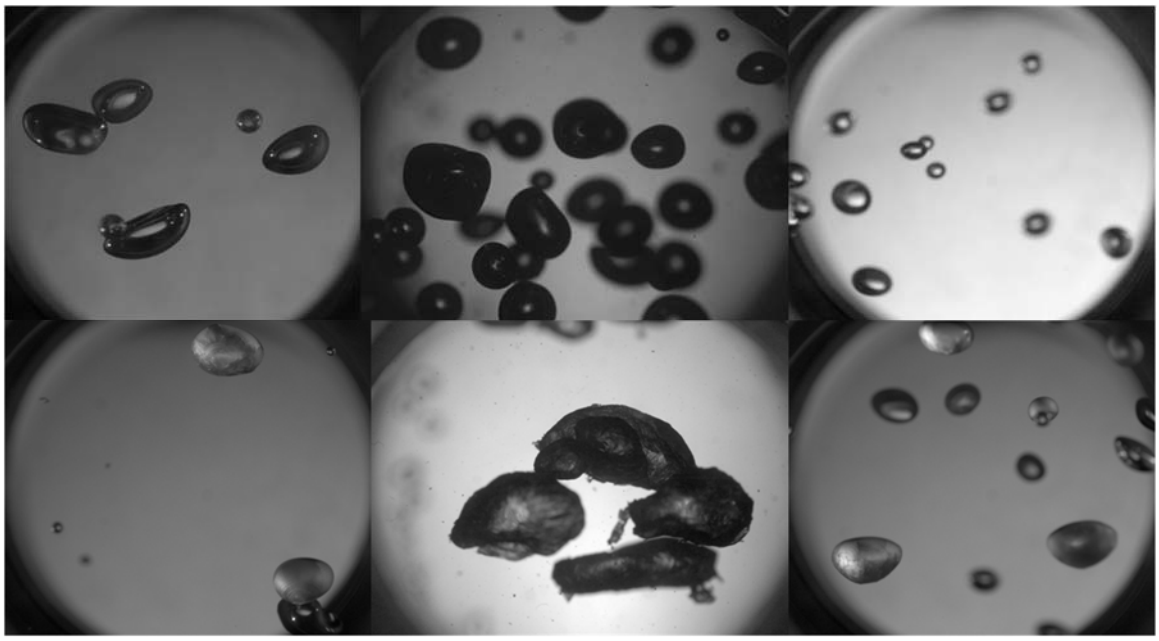

Figure 13: Bubble plumes in the HWTF (Phases I–II). Top: no hydrates. Bottom: hydrates.

However, hydrate identification during Phase I is made more difficult by dense optical fields with many bubbles either partially obscured or out of focus as shown in Figure 14 and Figure 15. Each bubble reflects and refracts images of other bubbles with their central bright regions noticeably present, making each bubble covered with bright spots. In the midst of tens or hundreds of bubbles and liquid oil droplets rising at 10–30 cm/s, identifying a hydrate-covered bubble may be difficult. A hydrate-covered bubble can be seen in the top right corner of Figure 14. In this example it is distinguished by the absence of multiple reflections.

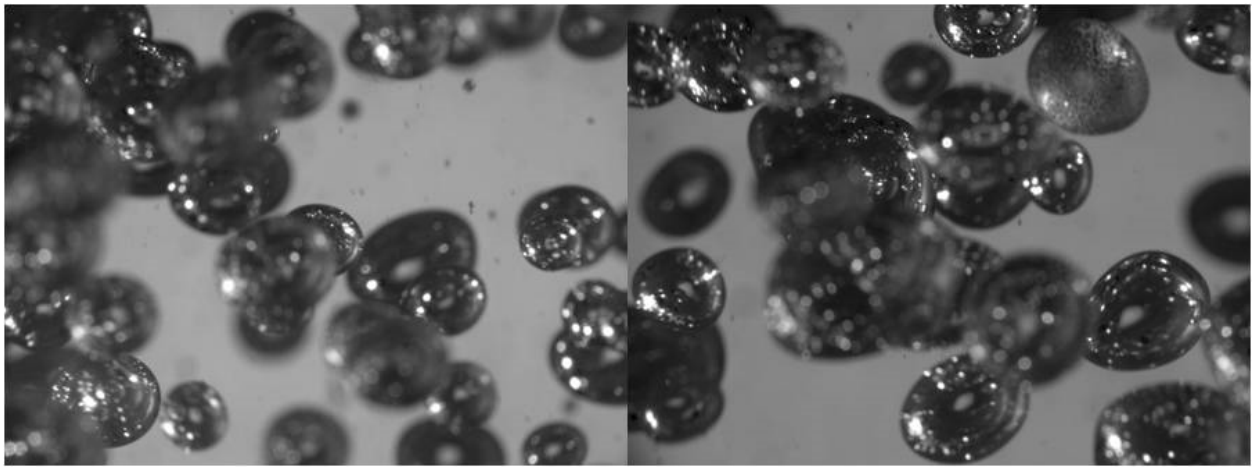

Figure 14: During Phase I, dense bubble plumes are optically difficult. The bright spots on each bubble are reflections of the side and back lighting off of other nearby bubbles. A hydrate covered bubble is hiding in the top right corner of the image at right.

Examples of focusing problems can be seen in Figure 15. This figure also shows how the combination of gray-scale values, perimeter shape, and the presence of hydrate flakes—all discussed in detail below—can be combined to unambiguously identify the presence of hydrate in such plumes.

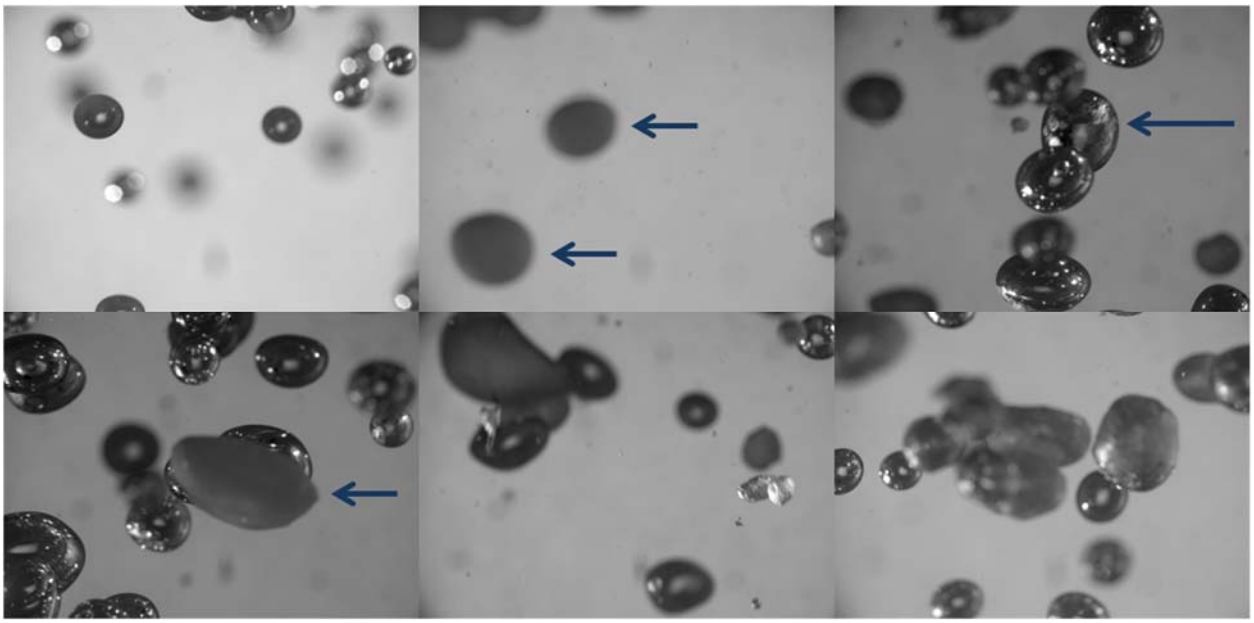

Figure 15: Bubbles are often out of focus in videos of dense bubble plumes simulating Phase I. Top left: no hydrates. Top middle: out of focus bubbles covered in hydrate. Top right: bubbles with no hydrate obscuring a bubble with a thin shell of hydrate. Bottom left: an out of focus hydrate-covered bubble in the foreground can definitely be identified by the sharp pointed outline but only probably by its gray appearance. Bottom middle and right: while many bubbles are out of focus, the multitude of bubbles that are gray, have textured lighting, have non-smooth jagged or pointed features, and the floating flakes overwhelmingly point to the presence of hydrate. The sharply-in-focus small white bubble in the bottom middle is unambiguously covered in hydrate.

An ideal location for hydrate identification is therefore Phase II, the transitional phase between dense bubble plumes and solitary bubbles. By locating a ROV immediately above the too-dense region of Phase I in the less-dense Phase II region, issues of bubbles being obscured or out of focus will be minimized, making hydrate identification easier. Figure 16 shows hydrate-covered bubbles in less-dense bubble plumes.

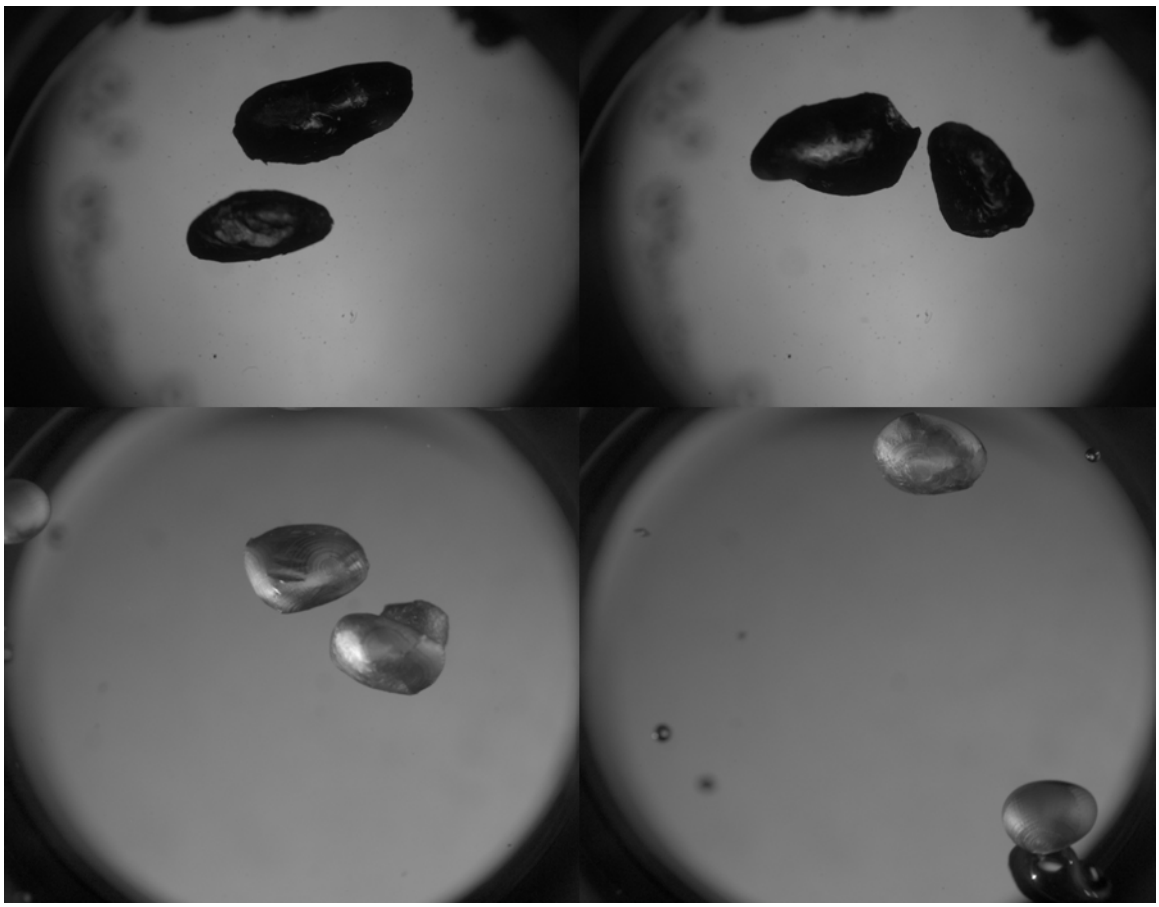

Figure 16: During Phase II, dense bubble plumes have thinned out and only a handful of bubbles are visible creating ideal conditions for hydrate identification. Hydrate can be seen in all four images.

4.1.4 Other Forms of Hydrate

While experiments at the HWTF primarily focused on hydrates on the surface of individual bubbles, hydrates could be seen in several other forms. At the highest driving energies, hydrate-covered bubbles rapidly shed flakes of solid hydrate from the hydrate surface (Figure 17). These flakes can be seen floating in the HWTF during some experiments (Figure 18). Very small hydrate particles are nearly-neutrally buoyant and have been used in the HWTF as streamline tracers (Lynn et al., 2014). During the Deepwater Horizon Macondo well disaster many such flakes can be seen in videos, but as noted above, it is not possible to identify them as being flotsam or hydrates without, e.g. collecting them and performing an additional measurement or test. However, clear signs of hydrate are flakes visibly shedding from a bubble as seen in Figure 17 and flakes large enough to have distinct ice-like surface texture such as Figure 18.

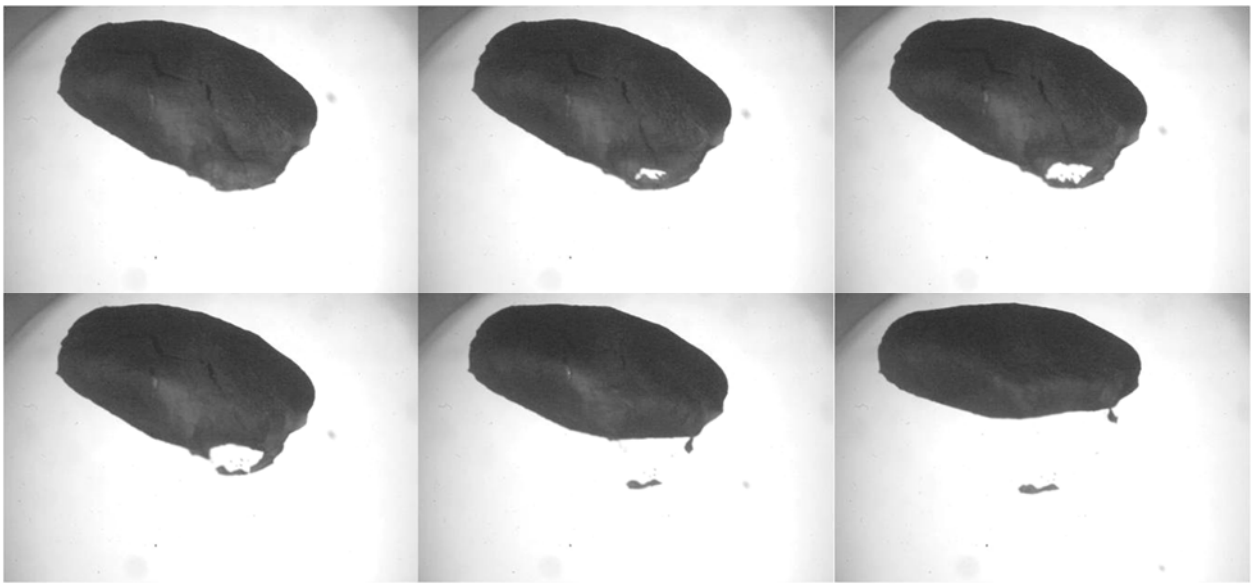

Figure 17: A hydrate flake shedding from a methane bubble.

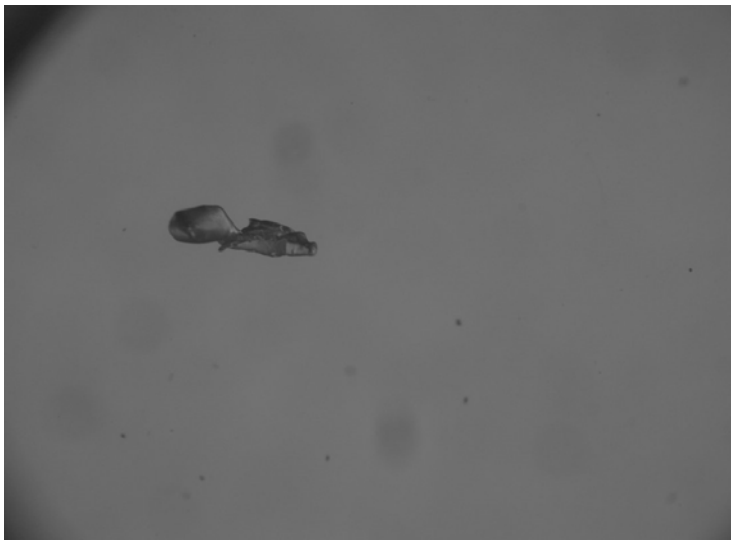

Figure 18: A large hydrate flake in the HWTF.

Experiments in the HWTF and reports from field ROVs warrant a note of caution. Hydrate preferentially forms on metal surfaces and in stagnant regions. In early experiments in the HWTF under hydrate-forming conditions, hydrate could form either in cutouts in the tapered inserts in the windowed viewing section (see Section 3.1) or in an inverted metal cup (Bubble Cap in Figure 7) that was used to form a bubble by coalescing smaller bubbles injected into it. Hydrate that has formed in the window cutouts is shown in Figure 19. Figure 20 shows a hydrate conglomerate that formed in the bubble cap. Scientific oceanographic field experiments must take similar elaborate precautions to avoid hydrate nucleation from gas accumulation by similar mechanisms on ROVs (MacDonald, 2011). Hydrates sticking to a ROV surface or on a ROV

camera should *not* be taken as indicating that hydrate is forming elsewhere in the leak where it would alter the fate of hydrocarbons.

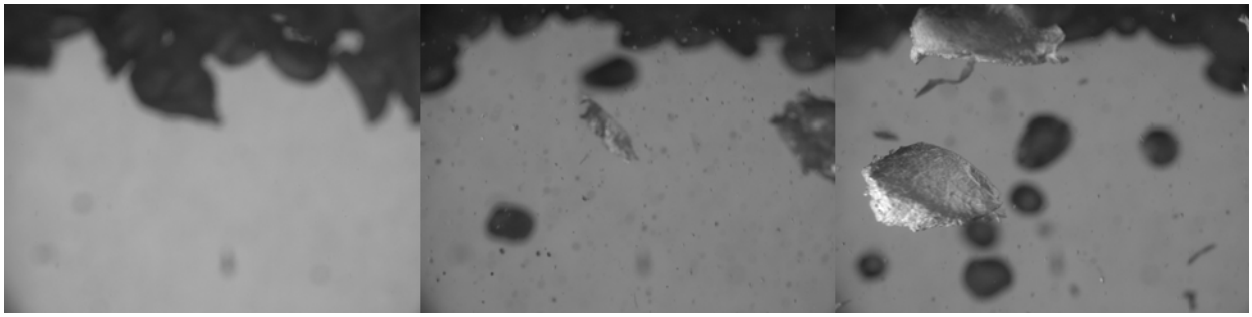

Figure 19: Three images of hydrates sticking to the upper surface of the HWTF viewing window cutout in a tapered plastic insert used for flow conditioning (see Section 3.1). Hydrate flakes and particles are present as well as hydrate-skinned bubbles.

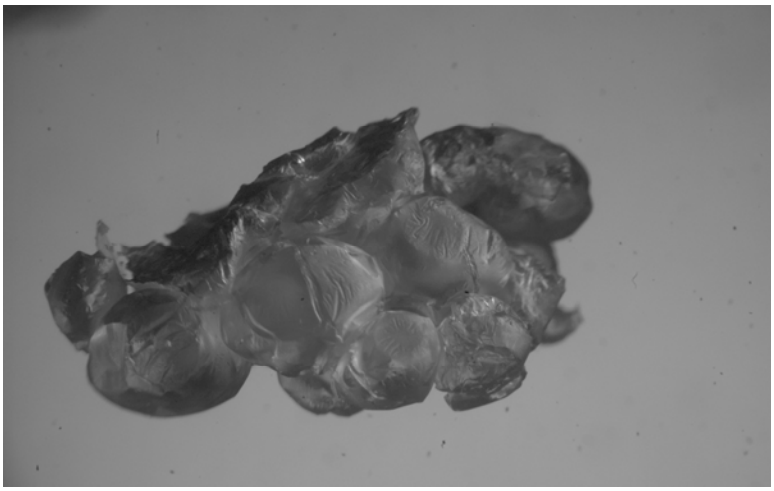

Figure 20: A hydrate cluster formed from many smaller gas bubbles in the HWTF metal cup used to collect small gas bubbles to form larger gas bubbles for HWTF single bubble experiments. Hydrate formed on each small gas bubble immediately as it contacted the metal cup. After gas bubbles completely covered the lower side of the metal cup, subsequent bubbles immediately formed hydrate upon contact with the hydrate-encrusted bubbles. The imprint of the metal cup and the breakage surfaces can be seen on the top surface.

4.1.5 Laboratory vs. Subsea Imaging

The images presented here were performed with a professional-grade high-speed video camera. In theory, the analyses can be performed with HDSDI video. Consumer-grade underwater digital cameras are capable of producing an HDSDI signal and much higher resolution still images (10–20 megapixels vs. the 4 megapixels here). High-speed video, 240 fps, is also available, though with significantly reduced image resolution. However, the sharpness and lack of blur in the images presented here required: (1) a quick shutter speed; (2) significant lighting; (3) optics

capable of focusing on a very small depth plane; and (4) a large low-noise CCD. Professional-grade digital and high-speed cameras are designed to solve these exact issues: lighting, focus, producing crisp clear images in challenging environments. During the response to a leak the video quality will be limited to whatever is available and can be deployed subsea. Standard video equipment is available on submersibles and ROVs. Advanced planning will be required to be able to deploy a camera capable of higher resolution, high-speed video in the deepsea, as well as the required lighting. Related research by Frank Shaffer at NETL aims to accurately determine leakage rates using high-speed video of fluids exiting leaking nozzles.

4.2 QUANTITATIVE VIDEO ANALYSIS

4.2.1 Overview and Challenges

While visual detection of hydrates is the simplest means of identification, quantitative analysis of bubbles can provide a more robust and sensitive means of determination. These analyses can be broadly assigned to two categories: those that can be performed on single images, e.g. detection of jagged hydrate crusts, and dynamic processes that require more complex analysis of a video sequence, e.g. bubble hydrodynamic frequency analysis.

4.2.2 Gray-scale

The most obvious difference to the eye in the images above is that non-hydrated bubbles appear black while hydrated bubbles appear gray to white. The formation of thick hydrate shells creates a significant change in bubble gray-scale values. Figure 21 shows that hydrate formation creates a step change in gray-scale values.

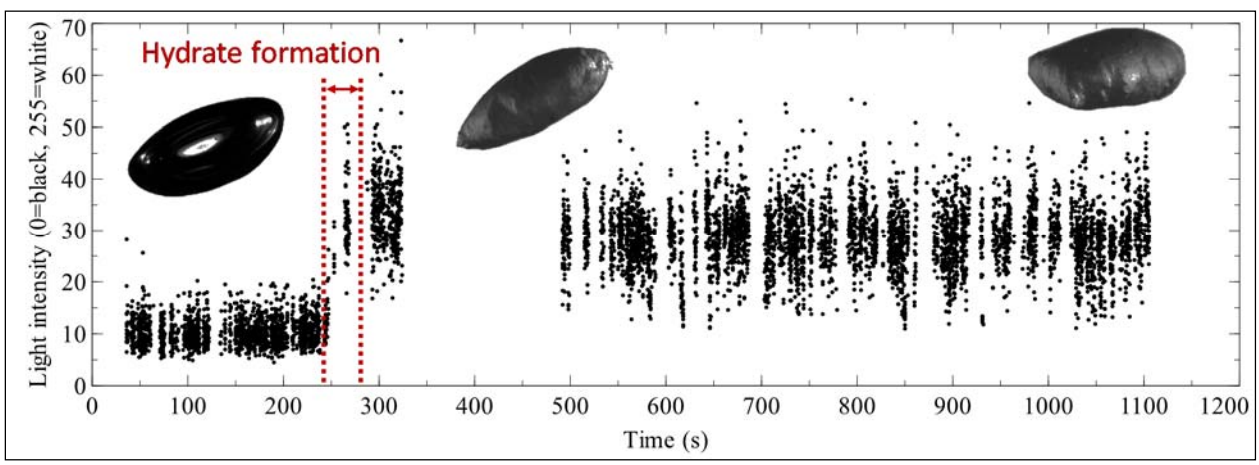

Figure 21: Gray-scale values change due to hydrate formation: the hydrate-free bubble is nearly black while the hydrates appear gray from reflected light. Experimental details are in Warzinski et al. (2014a).

While gray-scale identification is a simple measure, it requires that sufficient and consistent lighting has been provided. The HWTF includes significant back and side lighting to enable high-fidelity, high-speed images. In earlier images hydrated bubbles appeared dark (Figure 22, left), which was solved by increasing the amount of light entering the system (Figure 22, right).

Lighting issues should be addressable during system design and testing. Another complication is that bubbles at low thermodynamic-driving forces can have thinner shells that are translucent and do not alter the appearance of bubbles, which causes them to be relatively dark (e.g., Figure 12). This can be addressed by operating ROVs in Phases II and III and avoiding the transitional Phase IV region.

Figure 22: Methane bubbles covered in hydrate. Left: The earliest HWTF experiments had insufficient lighting and hydrate was difficult to see. Right: Later experiments used much more intense lighting to illuminate fine details.

4.2.3 Bubble Perimeter/Shape

The simplest visual indicator of hydrates is the jagged non-smooth features that are typically seen in HWTF experiments at conditions far inside the hydrate stability region (Figure 8, Figure 10, Figure 13, Figure 16, Figure 23).

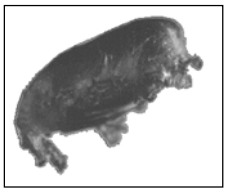

Figure 23: A hydrate-covered bubble with a very jagged perimeter.

Irregular shapes due to hydrate formation cause an increase in the perimeter of a bubble relative to a perfect oblate spheroid. The ratio of the actual perimeter to the perimeter of an ideal ellipse can be used to quantify deviations from a smooth bubble. Figure 24 shows that the perimeter ratio of a hydrate-free oblate spheroid bubble ranges from 1, a perfect ellipse, to a maximum of about 1.15 for larger bubbles, i.e. a perimeter 15% larger than would be expected for a perfect ellipse. By contrast, the hydrate-covered bubble shown at the top left of Figure 10 has a maximum perimeter that is about 40% larger than would be expected for a perfect ellipse.

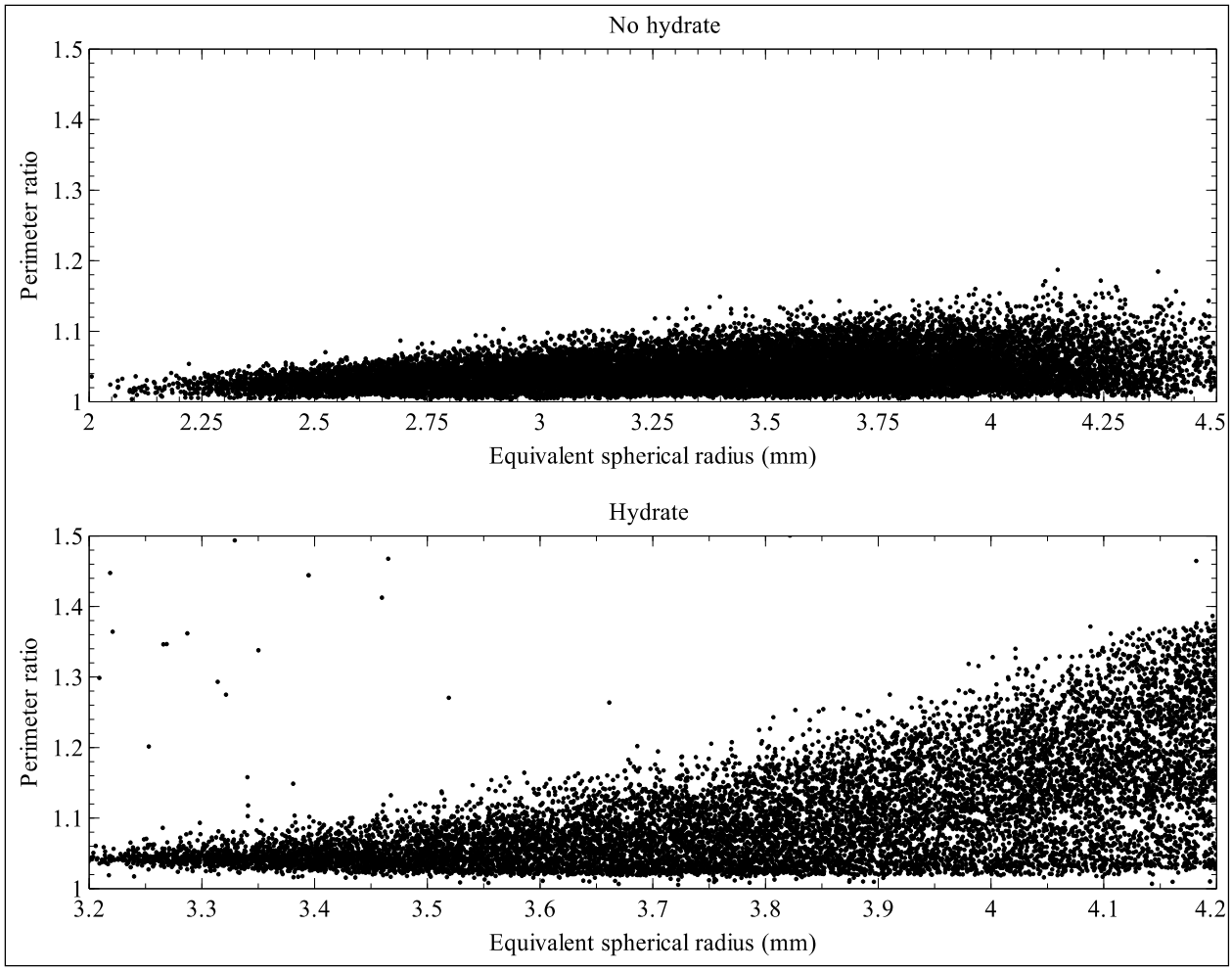

Figure 24: The ratio of the actual perimeter to the perimeter of an ideal ellipse vs. bubble size for bubbles with and without hydrate.

4.2.4 Bubble Rise Velocity

Bubble rise velocities decrease immediately after hydrate formation (Warzinski et al., 2014b). Figure 25 shows an example of hydrate-formation causing an immediate decrease in rise velocity of about 10% for a bubble of about 1-cm diameter. Figure 26 shows preliminary results for smaller bubbles that point to an even more marked decrease in rise velocity. This data set was generated using particle imaging velocimetry to measure rise velocities of freely rising hydrocarbon bubbles in the HWTF, i.e. with no counterflowing water.

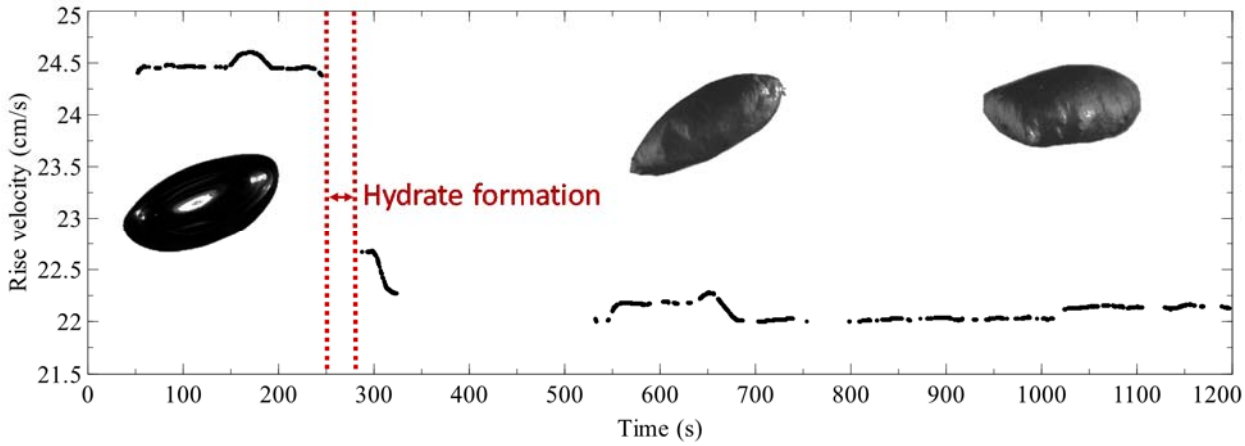

Figure 25: Rise velocity decreases approximately 10% after hydrate formation (Warzinski et al., 2014b). The moment that thick hydrate completely covers the bubble the rise velocity immediately drops and thus the rise velocity cannot be determined from the instantaneous flow rate of the counterflowing water.

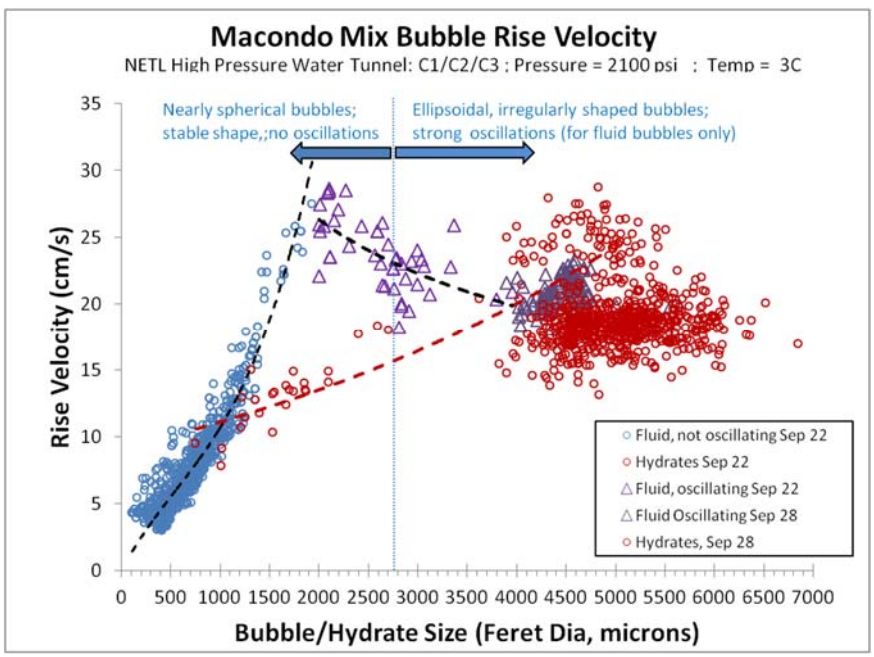

Figure 26: Preliminary results indicate that small hydrate-covered bubbles (<2.5 mm) have significantly decreased rise velocities.

4.2.5 Surface Dampening and Bubble Hydrodynamics

Experiments at the HWTF show that thermodynamic state controls surficial hydrate morphology and thickness (Warzinski et al., 2014b). Hydrate formation on the surface of a bubble dampens or prevents 1) bubble shape oscillations, 2) vortex-shedding induced surface deformations, and 3) surface capillary waves, all of which are related to bubble hydrodynamics. Therefore, sensitive and robust indicators of the presence of hydrate can be developed by using automated vision

analysis to quantify changes in the dynamics of bubble shape from surface and hydrodynamic alterations. This analysis requires high-speed contiguous video data for hydrodynamic frequency analysis to identify changes between hydrate-free and hydrate-covered bubbles. The preliminary results discussed below have been successful in quantifying the relevant processes in hydrate-free bubbles.

The equivalent spherical radius, R_e, of bubbles in HWTF experiments range between 1 and 6 mm and are oblate spheroids. Bubbles where R_e <0.5 mm are nearly spherical because surface tension dominates. Very large bubbles where R_e>10mm, are caps or half-spheres because buoyancy dominates. As a practical matter these larger bubbles are short lived in the ocean and typically break up into smaller bubbles. In between these two extremes bubbles are oblate spheroids, with the ratio of the horizontal to vertical axes increasing as the diameter increasing from 1 mm to 1 cm. In this intermediate regime surface tension is sufficient to keep bubbles intact; however rapid bubble rise due to buoyancy causes complex hydrodynamics that are coupled to surface motions. At this size range bubbles rotate as they rise, and rise in either a helical spiral or a zigzag motion induced by vortex shedding. As a result the projected image of a rising bubble, as viewed from a fixed camera, is a complex rotating ellipse with oscillating major and minor axes (shape oscillations) as well a travelling surface capillary wave. Figure 27 and Figure 28 show how the shape and appearance of oblate spheroid methane bubbles changes during a hydrodynamically-induced path oscillation.

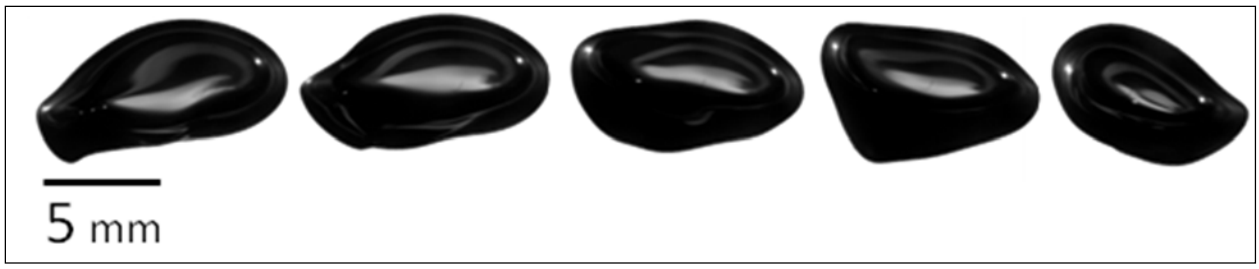

Figure 27: A sequential series of images showing one rotation of a 9-mm diameter oblate spheroid methane bubble. A surface wave can be seen traveling around the bottom surface of the bubble.

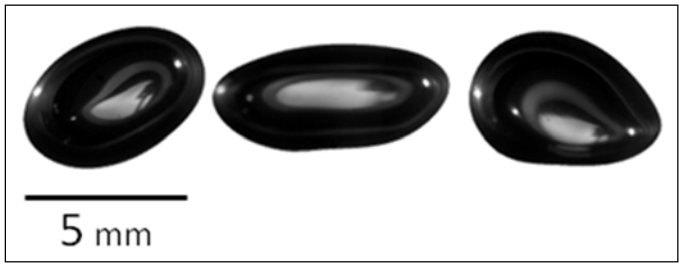

Figure 28: A sequential series of images showing half a rotation of a 6-mm diameter oblate spheroid methane bubble.

Hydrate forms as a flexible or rigid shell on the surface of a bubble and dampens the surface motion. Internal fluid motion can be seen by the eye in high speed videos of bubbles with only a

thin hydrate skin, with waves visibly deforming the solid surface in the same manner as a wave on a lake with only a thin veneer of ice. Thick hydrate skins are rigid and do not move from internal fluid rearrangement. Figure 29 shows a bubble with a thick hydrate skin rotating. The bubble shape is fixed, the visible notch in the first image goes out of view as the bubble rotates, but is unchanged for many minutes.

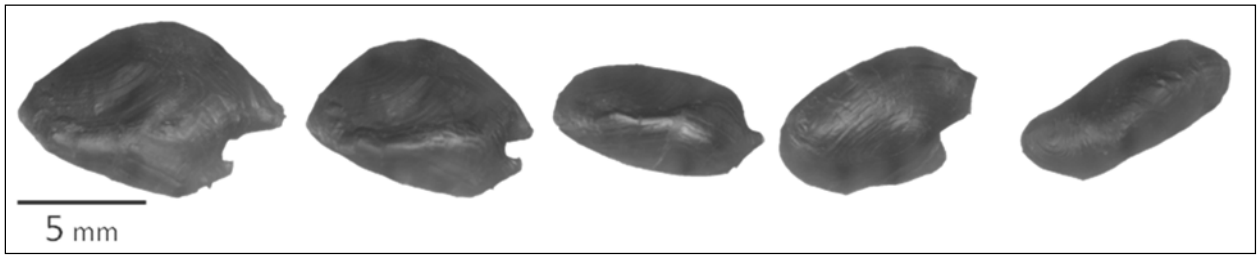

Figure 29: A sequential series of images showing the rotation of a hydrate-covered 7-mm diameter methane bubble.

A fixed camera, either the HWTF camera or a ROV camera, sees a two-dimensional (2-D) projection of the three-dimensional (3-D) bubble. While the volume of a bubble is unchanged between frames, the 2-D size varies as the bubble rotates. Simultaneously, bubble shape oscillations and capillary surface waves will cause the bubble size to appear to change from the perspective of the camera. All of these processes are linked to the helical or zigzag bubble rise and therefore changes in bubble radius should be sinusoidal. Hydrate causes surface dampening, which will reduce or eliminating bubble shape oscillations, surface capillary waves, and vortex shedding-induced surface deformations. Thus, it should be possible to identify hydrate by frequency and amplitude analysis of sinusoidal short-time variations in bubble radius.

The Allan variance measures the variance between sets of adjacent time-series of data of varying lengths of time, i.e. it quantifies high-frequency differences in data such as rapid bubble size changes. Additional details on Allan variance as applied to bubbles will be published in a manuscript currently under preparation. The Allan variance of bubble radius data reaches a local maximum corresponding to one-fourth of the bubble rotation frequency, with the amplitude proportional to a combination of shape oscillations, bubble rotation, and surface deviations from capillary surface waves. The data in Figure 30 show that the amplitude decreases as the bubble radius decreases for hydrate-free bubbles.

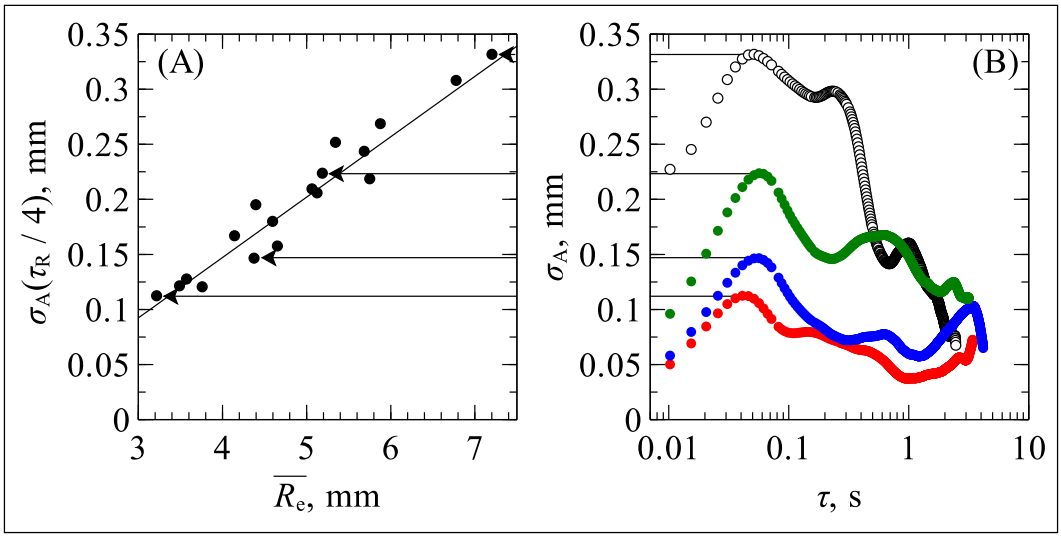

Figure 30: The maximum Allan variance, σA, of time-series bubble radius data decreases as the bubble size decreases for hydrate-free bubbles.

The next step in this analysis is to apply these methods to hydrate-covered bubbles. While this method requires a time series of quantitative bubble geometric data, it should also be much more sensitive to hydrate formation than analysis of single frames. Additionally, because it uses many hundreds or thousands of frames of data that are independent of exterior conditions such as lighting it should be more robust at hydrate identification.

4.3 CHEMICAL DETECTION METHODS

4.3.1 Hydrate Solubility

Hydrate forms in thermodynamic equilibrium with a gas. The thermodynamic conditions upon formation, including pressure, temperature, and relative proportions of hydrate formers and water, will determine the concentration of components in the hydrate phase. The hydrate will then be transported elsewhere in the deepsea before melting. As a result the concentrations of hydrate formers will be the same in the melt water as at formation. Dilution will occur as the hydrocarbon hydrate formers mix into the surrounding ocean; however, the ratio of hydrocarbons will remain the same. The aqueous solubility is limited by the least soluble hydrate former in proportion to the relative molar concentration of species in the hydrate. Figure 31 shows the solubility of hydrocarbons in the ocean. In the absence of hydrate each gas has a unique solubility. The formation of hydrate on gas bubbles results in a single shared solubility for the hydrate phase, locking the solubilities to the ratio of the hydrocarbons within the hydrate.

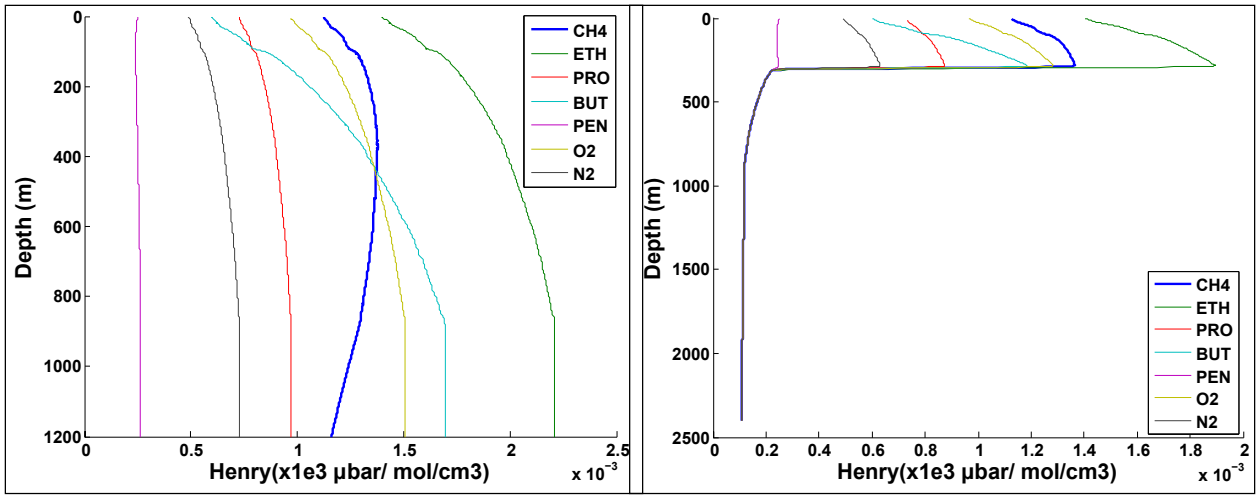

Figure 31: In the absence of hydrate, the solubility of each gas is independent (left). By contrast, hydrate dissolving into the ocean has a single fixed solubility (right) controlled by the least soluble hydrate-former when corrected for the relative molar concentration in the hydrate.

Locked ratios of light alkanes in the water column should therefore be a chemical signature of hydrate dissolution. Hydrate composition will change depending on the composition of the hydrate-forming gas. Thus, as the composition of leaking fluids changes with time, successive hydrate-skins on bubbles will transport different hydrate-former ratios. This could be advantageous in providing time-series data of changing leak compositions.

The instantaneous aqueous concentration at any given spatial location/depth in the ocean depends on melting from bubbles that had previously passed nearby and then diffused/diluted away from the passing gas bubble. More advantageous measurement locations can be chosen. As above, Phase I likely has too much variation, but the Phase II region should benefit from higher bubble density increasing the local aqueous gas concentrations. Density-driven intrusion layers and the bottom of the thermocline are also likely to be regions with melting hydrate leading to higher aqueous hydrocarbon concentrations.

4.3.2 Chemical Detection of Hydrates and Aqueous-phase Hydrocarbons

Aqueous hydrocarbon solubilities will depend on the mixture of hydrate-forming light alkanes in leaking fluids. Figure 32 and Figure 33 show calculations of the aqueous solubility of methane and a methane/ethane/propane mixture using NETL-WVU's thermodynamic model (Warzinski et al., 2004). Methane solubility at the 4°C typical of the deepsea is about 1,100–1,200 ppm. For a mixture of methane, ethane, and propane at the molar ratios found in Deepwater Horizon, the solubility is lower, only about 350–450 ppm. This corresponds to 300–400 ppm methane, 28–36 ppm ethane, and 15–20 ppm propane. Variations in the ratio of hydrate-forming gasses will result in different solubilities, so these values should be taken as representative of the order of magnitude of expected aqueous concentrations: 100s of ppm for methane, 10s of ppm for ethane, and single to low 10s of ppm for propane and other hydrate-forming hydrocarbons, isobutane and a handful of non-alkanes that are small enough to fit in hydrate cages. Thus, accurate chemical sensing of hydrocarbon ratios will require a sensor capable of measuring at ppm or

high ppb levels, while being robust to the difficulties of operating in the deepsea during an oil spill.

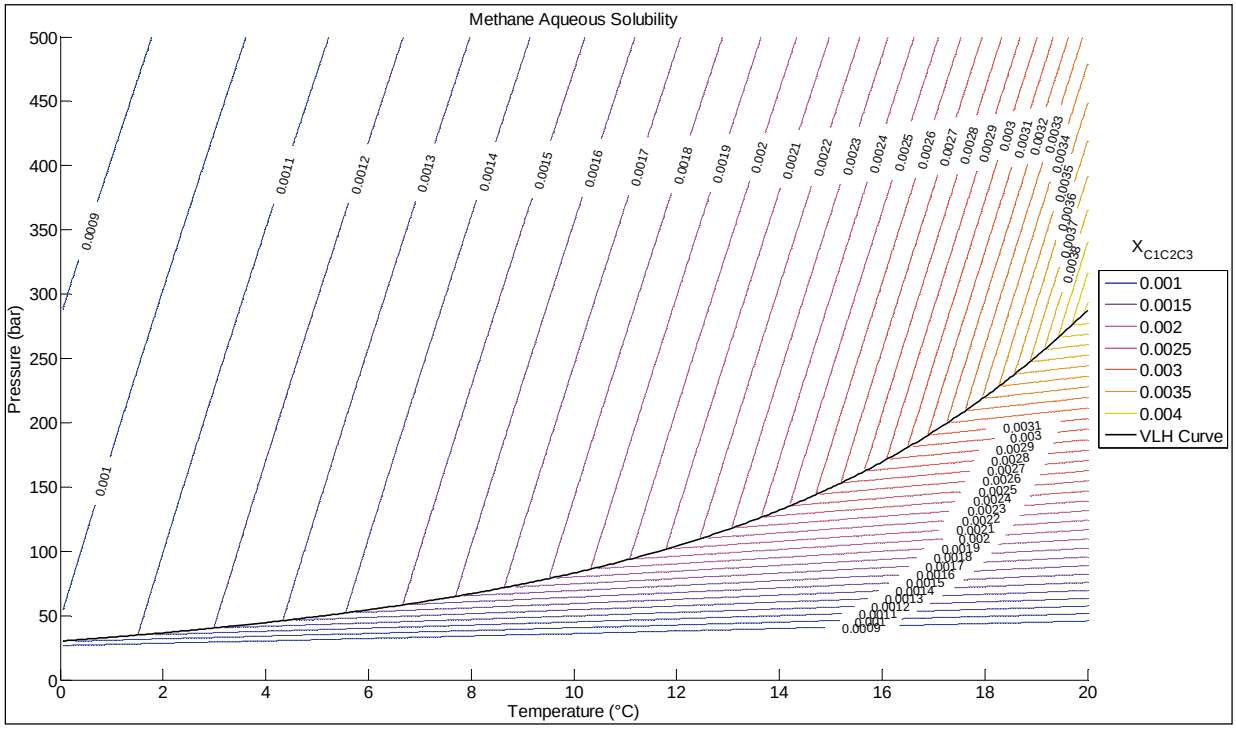

Figure 32: Aqueous solubility of methane calculated with NETL-WVU's thermodynamic model: above the black vapor-liquid water-hydrate (VLH) curve the solubility is controlled by hydrate in equilibrium with water, below the curve hydrate is thermodynamically unstable and the solubility is controlled by gas solubility.

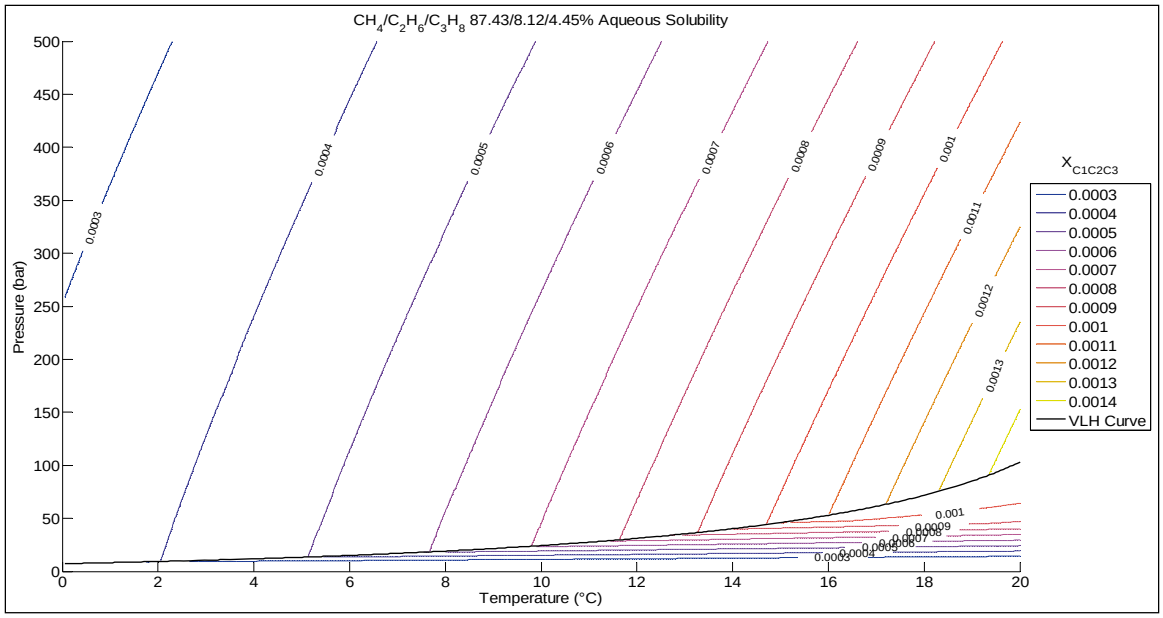

Figure 33: Aqueous solubility of a hydrocarbon mixture corresponding to the ratio of methane, ethane, and propane reported for Deepwater Horizon, and used as an illustrative ratio of light hydrocarbons. Calculations were performed with NETL-WVU's thermodynamic model.

4.4 FUTURE DETECTION METHODS

4.4.1 Acoustic Detection

Gas bubbles are commonly sized by looking at resonance frequency for a given diameter. For additional details consult the textbook, *The Acoustic Bubble*, by Timothy Leighton (Leighton, 1994). Hydrate on the surface acts to dampen surface waves, hence it will dampen the acoustic response. However, a sheen of oil would also dampen an acoustic wave traveling on the surface of a bubble. Furthermore, acoustic detection will be greatly complicated by the difficult environment. A careful set of laboratory and field experiments would be needed to calibrate acoustic measurements of hydrate-covered bubble to enable quantitative measurements. These experiments would likely also require an accurate non-invasive means of establishing hydrate shell thickness.

4.4.2 Raman Detection

Hydrates have known optical spectra that can be used for direct identification (Sloan and Koh, 2008). Hydrate molecular bonds absorb in the infrared, but infrared light rapidly attenuates in water. Raman spectroscopy can be used to identify hydrates and to measure aqueous-phase hydrocarbons (as discussed in Section 4.3), but requires specialized techniques such as coherent anti-Stokes Raman scattering (CARS) coupled to a waveguide to achieve sufficient signal. NETL and Pacific Northwest National Laboratory (PNNL) have proposed such a system to BSEE and further details are in that research proposal.

4.5 FUTURE WORK: THERMODYNAMICS

4.5.1 Current State of the Field

Accurate predictions of hydrate thermodynamics are critical to modeling the role of hydrates in deep-sea gas/oil leaks. Hydrate formation can only occur at depths deeper than the vapor-liquid water-hydrate (VLH) thermodynamic stability, while liquid water-hydrate (L_w-H) solubility/thermodynamics controls the dissolution rate of rising hydrate-encrusted gas bubbles.

Several academic and commercial software programs can accurately predict the VLH pressure/temperature condition for hydrate stability for a given hydrocarbon composition. Since the ocean temperature profile is easily measureable this is equivalent to predicting the depth for hydrate stability. Sloan and Koh (2008) have compiled a list of software as well as a lengthy treatment showing that for hydrocarbons and their mixtures model accuracy is as good as laboratory measurement accuracy, i.e. VLH thermodynamics can be accurately predicted.

4.5.2 Field Measurement Requirements

Hydrate thermodynamic models require accurate hydrocarbon mixture information. Deepwater Horizon showed that the composition of leaking gas and oil is important to many response actions, in particular stopping the leak and collecting leaking gas and oil, as well as long term physical, chemical, and biological predictions. Therefore, it was assumed that the composition of leaking gas and oil would be relatively rapidly determined. However, if composition varies during a leak then additional sampling would be necessary to update predictions of hydrate stability.

4.5.3 Aqueous Solubility Thermodynamics

As discussed above, the aqueous solubility of hydrate will determine the dissolution of gas bubbles and therefore where hydrocarbons are transported in the water column. The accuracy of model predications such as those made with WVU's thermodynamic code (Warzinski et al., 2004) could be confirmed with the limited aqueous hydrate solubility data for single hydrate formers including methane, ethane, propane, and carbon dioxide. However, no such data exist for hydrocarbon mixtures. A comprehensive set of experiments for several hydrocarbon gas mixtures would provide data to validate thermodynamic models. The HWTF includes a supporting laboratory that is capable of making thermodynamic measurements of the two-phase liquid water-hydrate system. This system has previously been used to measure the thermodynamics of carbon dioxide and methane and could be used to measure hydrocarbon mixtures. Such a set of experiments would also be ideal for calibrating a quantitative Raman system.

4.5.4 Hydrate Skin Composition

An additional complication arises from the potential for hydrate to form from a subset of the hydrocarbon/sour gas mixture contained in the bubble. That is, hydrate could preferentially incorporate more propane, for example, than would be expected relative to model predictions. At this time no measurements have been made of hydrate-skin composition and hence there are no data for comparison.

Experiments at the HWTF carefully control the gas mixture composition for the bulk aqueous phase composition as well as the gas bubble released in each experiment. At the present time however, the HWTF does not have instrumentation to measure the composition of hydrate skins. Because the ratio of hydrocarbons in the gas bubble and bulk water phase are identical in these experiments the hydrate thermodynamic model provided can be solved by WVU's predictions. This requires the assumption that the hydrate formed is in equilibrium with the aqueous phase, which is based on the observation that hydrate skins do not form at pressure/temperature/aqueous concentration conditions outside the Lw-H stability region. Directly measuring the hydrate skin composition would provide the last necessary measurement for a dissolution model.

Measuring the composition of hydrate on a relatively rapidly moving gas bubble is a significant challenge. Recent advances at NETL Raman laboratories enable rapid Raman signal acquisition such that rastering the bubble surface and the surrounding fluid would be possible. This would have the added benefit of providing an independent measurement of hydrocarbons in the aqueous phase, which is currently done by mass balance. The same technology could then be taken to the subsea for in situ hydrocarbon determination from an ROV/autonomous underwater vehicle (AUV).

4.5.5 Hydrogen Sulfide Thermodynamics

While most hydrate thermodynamics can be accurately predicted, an important exception to this is mixed H_2S/hydrocarbon hydrates, where limited laboratory data prevent accurate thermodynamic modeling (Ward et al., 2014). While this is presently a subject of active research by academia and industry (Mohammadi and Richon, 2013), laboratory measurements have been more limited due to the dangers of working with toxic H_2S. Gas mixtures containing H_2S have the potential to cause safety issues and thus require additional investigation.

The WVU aqueous solubility thermodynamic model can be extended to include H_2S by performing ab initio calculations and incorporating the results into the thermodynamic model. However, without thermodynamic measurements it is not possible to determine the model accuracy. Such experiments must necessarily be performed at specialized thermodynamic laboratories with an abundance of safety protocols. NETL's HWTF is permitted for operations with small quantities of H_2S and has supporting equipment to perform hydrate thermodynamic experiments. Thermodynamic modeling and measurements could be coupled to kinetic experiments at the HWTF to determine bubble dissolution mass transfer kinetic rates with and without hydrate. Ultimately this data could be incorporated into the bubble plume model. Such a project would be a natural successor to the present EPAct and BSEE projects, repeating many of the same experiments, but with hydrocarbon/sour gas mixtures in place of methane and hydrocarbon mixtures.

5. CONCLUSIONS

- Laboratory experiments at the NETL High Pressure Water Tunnel Facility have enabled high-speed videography of hydrate formation and hydrate skins on hydrocarbon gas bubbles.
- Unprecedented high fidelity images have shown previously unknown hydrate morphologies with complex linkages to bubble hydrodynamics and complex surface behavior.
- Hydrate is clearly visible in high-speed high definition video at the HWTF.
- Hydrate detection during a deepsea leak can be made by a human operator.
- Image quality is critical and requires careful system design of a deepsea video system in advance of any leak.
- Quantitative automated image analysis can provide several measures indicating the presence of hydrate including gray-scale values, rise velocity, and high frequency hydrodynamic/shape analysis.
- Future work points to the need for liquid water-hydrate thermodynamic measurements of hydrocarbon mixtures as well as hydrocarbon/sour gas mixtures.
- Development of a CARS and waveguide-enhanced Raman spectroscopy system would enable deepsea hydrate quantification and subsea hydrocarbon detection. Such a system would also enable laboratory determination of hydrate skin composition, improve dissolution experiment modeling enabling mixed hydrocarbon modeling, and would support thermodynamic measurements.

This page intentionally left blank.

6. REFERENCES

Adams, E. NOAA Deepwater Blowout Workshop, 2011.

Anderson, K.; Bhatnagar, G.; Crosby, D.; Hatton, G.; Manfield, P.; Kuzmicki, A.; Fenwick, N.; Pontaza, J.; Wicks, M.; Socolofsky, S.; Brady, C.; Svedeman, S.; Sum, A. K.; Koh, C.; Levine, J.; Warzinski, R. P.; Shaffer, F. Hydrates in the Ocean beneath, around, and above Production Equipment. *Energy & Fuels* **2012,** *26*, 4167–4176.

Clift, R.; Grace, J. R.; Weber, M. E. *Bubbles, drops, and particles*; Courier Dover Publications, 2005.

Fan, L.-S.; Tsuchiya, K. *Bubble wake dynamics in liquids and liquid-solid suspensions*; Butterworth-Heinemann Stoneham, 1990.

Haljasmaa, I. V.; Vipperman, J. S.; Lynn, R. J.; Warzinski, R. P. Control of a fluid particle under simulated deep-ocean conditions in a high-pressure water tunnel. *Review of Scientific Instruments* **2005,** *76*, 025111–11.

Leighton, T. *The Acoustic Bubble*; Academic Press, 1994.Lynn, R. J.; Haljasmaa, I. V.; Shaffer, F.; Warzinski, R. P.; Levine, J. S. A pitot tube system for obtaining water velocity profiles with millimeter resolution in devices with limited optical access. *Flow Measurement and Instrumentation* **2014**.

MacDonald, I. *Remote Sensing and Sea-Truth Measurements of Methane Flux to the Atmosphere (HYFLUX project)*; Texas A&M University-Corpus Christi, 2011.

Mohammadi, A. H.; Richon, D., Clathrate Hydrate Phase Equilibria for Carbonyl Sulfide, Hydrogen Sulfide, Ethylene, or Propane Plus Water System Below Water Freezing Point. *Chem Eng Commun* **2013,** *200*, 1635–1644.

NOAA. NOAA Deepwater Blowout Modeling Workshop, Sept 2011.

Rehder, G.; Leifer, I.; Brewer, P. G.; Friederich, G.; Peltzer, E. T., Controls on methane bubble dissolution inside and outside the hydrate stability field from open ocean field experiments and numerical modeling. *Marine Chemistry* **2009,** *114*, 19–30.

Sloan, E. D.; Koh, C. A.; Sum, A. *Natural gas hydrates in flow assurance*; Gulf Professional Publishing, 2010.

Sloan, Jr., E. D.; Koh, C. *Clathrate hydrates of natural gases*; CRC Press, 2008.

Solomon, E. A.; Kastner, M.; MacDonald, I. R.; Leifer, I. Considerable methane fluxes to the atmosphere from hydrocarbon seeps in the Gulf of Mexico. *Nature Geoscience* **2009,** *2*, 561–565.

Velaga, S. C. *Stability of Methane-Ethane-Propane Mixed Gas Hydrates under Deep Water Conditions*; West Virginia University, 2014.

Ward, Z. T.; Deering, C. E.; Marriott, R. A.; Sum, A. K.; Sloan, E. D.; Koh, C. A., Phase Equilibrium Data and Model Comparisons for H2S Hydrates. *Journal of Chemical & Engineering Data* **2014**.

Warzinski, R. P.; Anderson, B. J.; Haljasmaa, I.; Leifer, I.; Levine, J. S.; Lynn, R.; Shaffer, F.; Velaga, S. *The Role of Gas Hydrates during the Release and Transport of Well*

Fluids in the Deep Ocean, Final Report; National Energy Technology Laboratory, 2014a.

Warzinski, R. P.; Lynn, R. J.; Haljasmaa, I.; Zhang, Y.; Holder, G. D. Dissolution of CO2 drops and CO2 hydrate stability under simulated deep ocean conditions in a high-pressure water tunnel. Third Annual Conference on Carbon Capture and Sequestration, Alexandria, VA, 2004.

Warzinski, R. P.; Lynn, R.; Haljasmaa, I.; Leifer, I.; Shaffer, F.; Anderson, B. J.; Levine, J. S. Dynamic morphology of gas hydrate on a methane bubble in water: Observations and new insights for hydrate film models. *Geophysical Research Letters* **2014b**.

Warzinski, R. P.; Riestenberg, D. E.; Gabitto, J.; Haljasmaa, I. V.; Lynn, R. J.; Tsouris, C., Formation and behavior of composite CO2 hydrate particles in a high-pressure water tunnel facility. *Chemical Engineering Science* **2008,** *63*, 3235–3248.

Werdigier, J.; Fountain, H. Gas Leak on Offshore Platform Forces Evacuation in North Sea. *New York Times* March 27, 2012.

Jared Ciferno
Director
Strategic Center for Natural Gas and Oil
National Energy Technology Laboratory
U.S. Department of Energy

Maria Vargas
Deputy Director
Strategic Center for Natural Gas and Oil
National Energy Technology Laboratory
U.S. Department of Energy

Roy Long
Technology Manager
Strategic Center for Natural Gas and Oil
National Energy Technology Laboratory
U.S. Department of Energy

Elena Melchert
Program Manager
Oil and Gas Production
Office of Fossil Energy
U.S. Department of Energy

Cynthia Powell
Director
Office of Research and Development
National Energy Technology Laboratory
U.S. Department of Energy

Kevin Donovan
RES Program Manager
URS Corporation